

---

# 5 A Statistical Thermodynamic Approach to Hydrate Phase Equilibria

## INTRODUCTION AND OVERVIEW

The object of [Chapter 4](#) was to provide an overview of phase equilibria concepts, which are more easily obtained through phase diagrams and the approximate, historical methods. With Chapter 4 as background, the subject of the present chapter is the phase equilibrium calculation method that is both most accurate and most comprehensive.

The statistical thermodynamic method discussed here provides a bridge between the molecular crystal structures of [Chapter 2](#) and the macroscopic thermodynamic properties of Chapter 4. It also affords a comprehensive means of correlation and prediction of all of the hydrate equilibrium regions of the phase diagram, without separate prediction schemes for two-, three-, and four-phase regions, inhibition, and so forth as in Chapter 4. However, for a qualitative understanding of trends and an approximation (or a check) of prediction schemes in this chapter, the previous chapter is a valuable tool.

Section 5.1 presents the fundamental method as the heart of the chapter—the statistical thermodynamics approach to hydrate phase equilibria. The basic statistical thermodynamic equations are developed, and relationships to measurable, macroscopic hydrate properties are given. The parameters for the method are determined from both macroscopic (e.g., temperature and pressure) and microscopic (spectroscopic, diffraction) measurements. A Gibbs free energy calculation algorithm is given for multicomponent, multiphase systems for comparison with the methods described in Chapter 4. Finally, Section 5.1 concludes with *ab initio* modifications to the method, along with an assessment of method accuracy.

Section 5.2 shows the prediction method of phase diagrams of the major components of natural gas, namely methane, ethane, and propane hydrates and their mixtures at the common deep-ocean temperature of 277 K. Many of the commonly observed phenomena in natural gas systems are illustrated, while the power of the method is shown to go beyond that of Chapter 4, to illustrate future needs.

The method presented in this chapter serves as a link between molecular properties (e.g., cavities and their occupants as measured by diffraction and spectroscopy) and macroscopic properties (e.g., pressure, temperature, and density as measured by pressure guages, thermocouples, etc.) As such Section 5.3 includes a brief overview of molecular simulation [molecular dynamics (MD) and Monte Carlo (MC)] methods which enable calculation of macroscopic properties from microscopic parameters. [Chapter 2](#) indicated some results of such methods for structural properties. In Section 5.3 molecular simulation is shown to predict qualitative trends (and in a few cases quantitative trends) in thermodynamic properties. Quantitative simulation of kinetic phenomena such as nucleation, while tenable in principle, is prevented by the capacity and speed of current computers; however, trends may be observed.

At the onset, it should be noted that the method presented here has been the subject of several recent theses. The reader is sure to gain additional insights from the thesis of Ballard (2002) who composed the revised method on the endpapers CD. A summary of the method is detailed in series of five publications, four by Ballard and Sloan (2002a,b; 2004a,b) and one by Jager et al. (2003). One major future direction of such calculations is indicated in Section 5.1.9 where the recent *ab initio* calculation methods of Cao (2002), Klauda (2003), and Anderson (2005) are discussed.

Since the statistical thermodynamics method is too involved for hand calculation, a computer program is provided on the CD accompanying this book. The use of the program is discussed in a preliminary way in each of the sections of the chapter, beginning in Section 5.2. A detailed User's Guide, which includes a description of the program, together with input data and illustrations, is provided in the CD which accompanies this book, and a User's Tutorial is included in [Appendix A](#). It is recommended that the reader first try the examples in Appendix A to become familiar with the program, referring to the more comprehensive CD User's Guide as needed.

While the method of the present chapter may appear comprehensive, the reader is cautioned that the calculation is limited by the available data, as in any prediction method. For each region of phase equilibrium prediction, the limitations on both the accuracy and data availability are discussed. The methods presented are useful for interpolations between available data sets. The reader is urged to use caution for extrapolations beyond the data range. Further experiments may be required in order to appropriately bound the  $P$ - $T$  conditions of interest.

## 5.1 STATISTICAL THERMODYNAMICS OF HYDRATE EQUILIBRIA

After the determination of the hydrate crystal structures in the early 1950s, it was possible to generate theories for equilibria of macroscopic properties based upon microscopic properties. With the knowledge of distinguishable cavities, each containing at most one guest particle, came the ability to describe the distribution of the guest particles via statistics (e.g., "How many ways can  $M$  indistinguishable particles be distributed in  $L$  distinguishable boxes with at most one particle per box?"). The resulting improvement in theoretical ability led to a more accurate

calculation method. Currently, the calculation of hydrate equilibria is the best exemplar of the industrial use of statistical thermodynamics on a routine basis.

The initial model was generated by Barrer and Stuart (1957), with a more accurate method by van der Waals and Platteeuw (1959), who are considered the founders of the method. In the present section the latter model is substantially expanded by Ballard (2002), as follows:

- 5.1.1 Grand Canonical Partition Function for Water
- 5.1.2 The Chemical Potential of Water in Hydrates
- 5.1.3 The Langmuir Adsorption Analogy
- 5.1.4 Relating the Langmuir Constant to Cell Potential Parameters
- 5.1.5 Activity Coefficient for Water in the Hydrate
- 5.1.6 Defining the Hydrate Fugacity and Reference Parameters
- 5.1.7 The Gibbs Free Energy Method
- 5.1.8 Accuracy of CSMGem Compared to Commercial Hydrate Programs
- 5.1.9 *Ab Initio* Methods and van der Waals and Platteeuw Methods

The first two of the above sections are a simplification and slight expansion of the derivation from the review article by van der Waals and Platteeuw (1959). They were written assuming that the reader has a minimal background in statistical thermodynamics on the level of an introductory text, such as that of Hill (1960), McQuarrie (1976), or Rowley (1994). The reader who does not have an interest in statistical thermodynamics may wish to review the basic assumptions in Sections 5.1.1 and 5.1.4 before skipping to the final equations and the calculation prescription in Section 5.2.

The derivation is a primary example of application of first principles in statistical thermodynamics, to link both microscopic and macroscopic domains for practical applications. For the reader's convenience, Table 5.1 gives the nomenclature used in Sections 5.1.1 and 5.1.2 as well as a listing (in parentheses) of the equations in which each term first appears.

### 5.1.1 Grand Canonical Partition Function for Water

To develop the model, it was necessary to make four fundamental assumptions based upon structure, stated as follows:

1. The host molecules' contribution to the free energy is independent of the occupation of the cavity. This assumption also implies that encaged molecules do not distort the cavity.
2. Each cavity can contain at most one guest molecule, which cannot diffuse from the cavity.
3. There are no interactions of the guest molecules, that is, the energy of each encaged guest molecule is independent of the number and types of other guest molecules.
4. No quantum effects are needed; classical statistics are valid.

**TABLE 5.1**  
**Nomenclature for Chapter 5**

Term	Definition	First equation
$A^\beta$	Helmholtz free energy of empty host lattice	(5.1)
$f_J$	Fugacity of a molecule of type $J$	(5.22c)
$g_J$	molar Gibbs free energy of component $J$	(5.28)
$N_{Ji}$	Number of solute (guest) molecules of type $J$ within type $i$ cavity	(5.2)
$N_W$	Number of host (water molecules)	(5.2)
$Q$	canonical partition function for host lattice	(5.4)
$q_{Ji}$	Partition function of a $J$ molecule in a type $i$ cavity	(5.3)
$y_k$	Stability variable	(5.42)
$\theta_{ki}$	Probability of finding a molecule of type $k$ in a cavity of type $i$	(5.17)
$\lambda_J$	Absolute chemical activity of guest molecule $J$	(5.5b)
$v_i$	Number of type $i$ cavities per water molecule (for cavity $i = S, M, L$ ; $S = 5^{12}, M = 4^3 5^6 6^3$ , $L_1 = 5^{12} 6^2, L_2 = 5^{12} 6^4, L_H = 5^{12} 6^8$ )	(5.2)
	<b>sI:</b> $v_S = 1/23, v_{L1} = 3/23; sII:$ $v_S = 2/17, v_{L2} = 1/17;$ <b>sH:</b> $v_S = 3/34, v_M = 2/34; v_{LH} = 1/34)$	
$\mu_J$	Chemical potential of component $J$	(5.5a)
$\Xi$	Grand canonical partition function for the guest–host ensemble	(5.5)

#### Subscripts and superscripts

$H$	Hydrate
$i$	Type of cavity
$I$	Ice
$J$	Type of guest molecule ( $1 \leq J \leq M$ )
$M$	Total number of possible guest components in the mixture
$\beta$	Property of the empty hydrate crystal
$o$	Standard state

As a convenient starting point for the model, the grand canonical partition function is developed from the canonical partition function, to incorporate the above assumptions. The canonical partition function is written as the product of three factors: the water lattice, the guest distribution within the cages, and the states of the guest molecules themselves assuming that they behave as ideal gas molecules, as follows:

*Factor 1:* The exponential of the empty water lattice Helmholtz free energy divided by  $kT$ , where  $k$  is Boltzmann's constant,

$$\exp(-A^\beta/kT) \quad (5.1)$$

*Factor 2:* The number of ways to distribute the indistinguishable guest molecules of type  $J$  in distinguishable cavities of type  $i$ , with an upper limit of one guest per cavity.

If we choose only one species of guest ( $N_{J,i} = N_{1,i}$ ) and define  $L$  as the number of boxes, then we obtain the statistical permutation formula for the number of ways  $N_{1,i}$  indistinguishable objects can be placed in  $L$  distinguishable boxes with at most one object per box.

$$\frac{L!}{(L - N_{1,i})!N_{1,i}!} \quad (5.2a)$$

In this case, however, there are  $v_i N_W$  distinguishable boxes of type  $i$  and we wish to distribute  $N_{J,i}$  indistinguishable objects, with no more than one object per box, so Equation 5.2a is modified to obtain the second factor in the canonical partition function as

$$\frac{(v_i N_W)!}{(v_i N_W - \sum_J N_{J,i})! \prod_J N_{J,i}!} \quad (5.2b)$$

*Factor 3:* The product of all individual particle partition functions,  $q_{J,i}$ , raised to the number of  $J$  particles in a type  $i$  cavity,  $N_{J,i}$

For the third factor, the analogy is an ideal gas mixture of  $N_1$  molecules of type 1 and  $N_2$  molecules of type 2, so that the canonical partition function for the ideal gas mixture is

$$Q(N_1, N_2, V, T) = \frac{q_1^{N_1} q_2^{N_2}}{N_1! N_2!} \quad (5.3a)$$

where the factorial product in the denominator accounts for the inability to distinguish among the molecules. In the clathrate, however, the molecules are distinguished by the cage they occupy, eliminating any need for  $N_1!N_2!$  in the denominator. Thus the third product term in the canonical partition function becomes

$$\prod_J q_{J,i}^{N_{J,i}} \quad (5.3)$$

Multiplying all three factors of Equations 5.1, 5.2b, and 5.3 together over type  $i$  cavities, the canonical partition function was obtained by van der Waals and Platteeuw:

$$Q = \exp\left(\frac{-A^\beta}{kT}\right) \prod_i \left[ \frac{(v_i N_W)!}{(v_i N_W - \sum_J N_{J,i})! \prod_J N_{J,i}!} \prod_J q_{J,i}^{N_{J,i}} \right] \quad (5.4)$$

We must use the grand canonical partition function  $\Xi$  because  $N$  (a natural variable to  $Q$ ) cannot be held constant with the insertion of guests in the hydrate. To obtain  $\Xi$  from the canonical function  $Q$ , we use the standard statistical mechanics transformation

$$\Xi = \sum_N Q e^{\mu N / kT} \quad (5.4a)$$

and since the chemical potential  $\mu$  is related to the absolute activity  $\lambda$  by

$$\mu = kT \ln \lambda \quad \text{or} \quad \lambda = e^{\mu / kT} \quad (5.4b)$$

then we can multiply Equation 5.4 by the product of the activity of each molecule raised to the number of molecules of type  $J$  in type  $i$  cavities, as

$$\lambda_A^{N_{A,1}} \lambda_A^{N_{A,2}} \dots \lambda_B^{N_{B,1}} \lambda_B^{N_{B,2}} \dots \lambda_M^{N_{M,1}} = \prod_i \prod_J \lambda_J^{N_{J,i}}$$

and sum over all values of  $N_{J,i}$ , to obtain the grand canonical partition function

$$\Xi = \exp\left(\frac{-A^\beta}{kT}\right) \sum_{N_{J,i}} \prod_i \left\{ \frac{(v_i N_W)!}{(v_i N_W - \sum_J N_{J,i})! \prod_J N_{J,i}!} \prod_J q_{J,i}^{N_{J,i}} \lambda_J^{N_{J,i}} \right\} \quad (5.5)$$

Consider the summation term in Equation 5.5 for one type of cavity ( $i = 1$ ) and for two types of guests ( $J = A, B$ ), for example, mixtures of C<sub>3</sub>H<sub>8</sub>(A) + i-C<sub>4</sub>H<sub>10</sub>(B) in 5<sup>12</sup>6<sup>4</sup> cavities:

$$\sum_{N_A} \sum_{N_B} \frac{(v_1 N_W)!}{(v_1 N_W - N_A - N_B)! N_A! N_B!} q_A^{N_A} q_B^{N_B} \lambda_A^{N_A} \lambda_B^{N_B} (1)^{(v_1 N_W - N_A - N_B)} \quad (5.5a)$$

with the final unity factor as the partition function for the empty cavity. Note also that the empty cavity has

$$\mu^\beta = 0, \quad \therefore \lambda^\beta = 1$$

Equation 5.5 may be simplified using the multinomial theorem from mathematics:

$$(x_1 + x_2 + \dots + x_m)^N = \sum_{N=\sum_1^m n_i} \frac{N!}{n_1! n_2! \dots n_m!} x_1^{n_1} x_2^{n_2} \dots x_m^{n_m} \quad (5.6)$$

When we consider the analogy between Equation 5.5a and the right-hand side of Equation 5.6 we obtain, from Equation 5.5a

$$(1 + q_A \lambda_A + q_B \lambda_B)^{v_1 N_W} \quad (5.5b)$$

So we have a product of terms, such as in Equation 5.5b, one for each cavity type  $i$ . Equation 5.5 then becomes simplified to its final form

$$\Xi = \exp\left(\frac{-A^\beta}{kT}\right) \prod_i \left(1 + \sum_J q_{J,i} \lambda_J\right)^{v_i N_W} \quad (5.7)$$

### 5.1.2 The Chemical Potential of Water in Hydrates

Our aim is to derive the chemical potential of water to enable phase equilibria calculations. Note that, while Equation 5.7 is the grand canonical partition function ( $\Xi^{\text{guest}}$ ) and with respect to the solute (guest) molecule, it is the canonical partition function ( $Q^{\text{host}}$ ) with respect to the host (water) because  $\lambda^\beta = 1$ , so that we have

$$\Xi^{\text{combined}} = Q^{\text{host}} \Xi^{\text{guest}}$$

or

$$kT \ell n \Xi^{\text{combined}} = kT \ell n Q^{\text{host}} + kT \ell n \Xi^{\text{guest}} \quad (5.8)$$

Now, using the letter “h” to denote the host, and “g” to denote the guest, each of the partition functions in Equation 5.8 can be related to their macroscopic thermodynamic properties in the usual way (see [McQuarrie](#), 1976, p. 58) as

$$d(kT \ell n Q^h) = -dA^h = S^h dT + PdV^h - \mu_W^h dN_w \quad (5.9)$$

and

$$d(kT \ell n \Xi^g) = d(PV^g) = S^g dT + PdV^g + \sum_J N_J d\mu_J \quad (5.10)$$

Since entropy and volume are extensive properties, they can be combined,

$$S = S^g + S^h \quad \text{and} \quad V = V^g + V^h$$

so that adding Equations 5.9 and 5.10 results in a revised form of Equation 5.8 as

$$d(kT \ell n \Xi^{\text{combined}}) = SdT + PdV + \sum_J N_J d\mu_J - \mu_W dN_W \quad (5.11)$$

By dropping the superscript “combined,” taking the left-most derivative, and using  $d\mu_J = kT d\ell n \lambda_J$  on the right, we get:

$$kT d\ell n \Xi = (-k \ell n \Xi + S)dT + PdV + \sum_J kTN_J d\ell n \lambda_J - \mu_W^H dN_W \quad (5.12)$$

With the development of Equation 5.12 relating the partition function and the macroscopic properties, all of the macroscopic thermodynamic properties may be derived from Equation 5.7. For example, differentiating  $\ln \Xi$  with respect to the absolute activity ( $\lambda$ ) of  $J$ , provides the total number of guest molecules “ $J$ ” over all the cavities  $i$

$$N_J = \sum_i N_{J,i} = \lambda_J \left( \frac{\partial \ell n \Xi}{\partial \lambda_J} \right)_{T,V,N_W,\lambda_{k \neq J}} \quad (5.13)$$

In Equation 5.13 the logarithm of  $\ln \Xi$  is obtained from Equation 5.7, as

$$\ln \Xi = -\frac{A^\beta(T, V, N_W)}{kT} + \sum_i v_i N_W \ln \left( 1 + \sum_J q_{J,i} \lambda_J \right) \quad (5.14)$$

to yield the total number of guest molecules  $N_k$  as

$$N_J = \sum_i \left( \frac{v_i N_W q_{J,i} \lambda_J}{1 + \sum_J q_{J,i} \lambda_J} \right) \quad (5.15)$$

Since  $N_J$  must be a linear, homogeneous function of  $v_i$ , the number of cavities of different types per water molecule, it follows from Equation 5.15 that  $N_J = \Sigma N_{J,i}$  and

$$N_{J,i} = \frac{v_i N_W q_{J,i} \lambda_J}{(1 + \sum_J q_{J,i} \lambda_J)} \quad (5.16)$$

Equation 5.16 may be used to determine the simple probability ( $\theta_{J,i}$ ) of finding a molecule of type  $J$  in a cavity of type  $i$ . This value may be obtained by dividing the number of molecules of  $k$  in cavity  $i$  by the total number of cavities of type  $i$ ,  $v_i N_W$

$$\theta_{J,i} = \frac{N_{J,i}}{v_i N_W} = \frac{q_{J,i} \lambda_J}{(1 + \sum_J q_{J,i} \lambda_J)} \quad (5.17)$$

The chemical potential of the host  $\mu_W^H$  may also be obtained from Equation 5.12 as

$$\frac{\mu_W^H}{kT} = - \left( \frac{\partial \ln \Xi}{\partial N_W} \right)_{T,V,\lambda_J}$$

so that, from Equation 5.14

$$\frac{\mu_W^H}{kT} = \frac{\mu_W^\beta}{kT} - \sum_i v_i \ln \left( 1 + \sum_J q_{J,i} \lambda_J \right) \quad (5.18)$$

Equations 5.17 and 5.18 are important because they enable the determination of the hydrate composition and the chemical potential of the hydrated water as a function of variables ( $T, V, N_W, \lambda_1, \lambda_M$ ).

Equation 5.17 may be simplified somewhat by finding expressions for the absolute activity  $\lambda_J$  and the individual particle partition function  $q_{J,i}$  in terms of experimentally measured or fitted parameters. To achieve such a simplification, we first consider the chemical potential of an ideal gas and its relation to the particle partition function.

For an ideal gas, the canonical partition function  $Q$  may be written as

$$Q = \frac{1}{N!} q^N$$

and the ideal gas chemical potential  $\mu$  is calculated by

$$\mu = -kT \left( \frac{\partial \ln Q}{\partial N} \right)_{T,V} = -kT \ell \ln \frac{q}{N}$$

where separability may be assumed for the individual particle partition function  $q$  into a translational part and a second part containing the internal modes of energy, that is,  $q = q_{\text{trans}} q_{\text{int}}$  with:

$$\frac{q_{\text{trans}}}{N} = \left( \frac{2\pi mkT}{h^2} \right)^{3/2} \frac{V}{N}$$

where the square root of the quantity in parentheses is called the mean thermal de Broglie wavelength. For an ideal gas  $V/N = kT/P$ , therefore

$$\mu = -kT \ell \ln \left[ \left( \frac{2\pi mkT}{h^2} \right)^{3/2} kT \right] - kT \ell \ln q_{\text{int}} + kT \ell \ln P \quad (5.19)$$

and since the chemical potential is normally defined in reference to a standard chemical potential  $\mu^\circ$  as

$$\mu = \mu^\circ(T) + kT \ell \ln P \quad (5.20)$$

the identity can be made between the standard chemical potential with the first two terms on the right of Equation 5.19 as

$$\mu^\circ = -kT \ell \ln \left[ \left( \frac{2\pi mkT}{h^2} \right)^{3/2} kT \right] - kT \ell \ln q_{\text{int}}$$

Without the standard chemical potential, Equation 5.19 becomes in terms of absolute chemical potential ( $\mu = kT \ell \ln \lambda$ ),

$$\mu = kT \ell \ln \frac{P}{kT(2\pi mkT/h^2)^{3/2} q_{\text{int}}}$$

or for the absolute activity  $\lambda$

$$\lambda = \frac{P}{kT(2\pi mkT/h^2)^{3/2} q_{\text{int}}}$$

The absolute activity and the individual particle partition function may be taken into account through a constant  $C_{J,i}$ , defined as

$$C_{J,i} \equiv \frac{q_{J,i} \lambda_J}{P_J} = \frac{q_{J,i}}{kT(2\pi mkT/h^2)^{3/2} q_{\text{int}}} \quad (5.21)$$

Note that the denominator of Equation 5.21 contains the internal portion of the particle partition function and the ideal gas contribution, so that the division indicated accounts for the nonideal gas effect. When Equation 5.21 is put into Equation 5.17,  $\theta_{J,i}$ , the fractional filling of cavity  $i$  by a type  $J$  molecule, is obtained:

$$\theta_{J,i} = \frac{C_{J,i}P_J}{1 + \sum_J C_{J,i}P_J} \quad (5.22a)$$

For an ideal gas Equation 5.22a may be considered as elementary probability of cavity  $i$  occupation by molecule  $J$ . This is one of the most useful equations in the method of hydrate prediction, and it may also be recognized as the Langmuir isotherm. If the equation were written for one guest component  $J$ , it would contain the Langmuir constant  $C_{J,i}$  as the only unknown for a given pressure and fraction of the cavities filled (or fraction of monolayer coverage).

Equation 5.21 shows that the Langmuir constant is a direct function of the particle partition function within the cavity  $q_{J,i}$ ; in particular  $C_{J,i}$  contains the nonideal gas translation term. When the fluid in equilibrium with the hydrate is a nonideal gas, the pressure of component  $J$  in Equation 5.22a is replaced with its fugacity,  $f_J$ .

With such corrections, Equation 5.22a finds many uses in the calculation of hydrate properties. The equation relies on the fitting of the Langmuir constant  $C_{J,i}$  to experimental hydrate conditions. The method of relating the Langmuir constant to experimental conditions is given in Section 5.1.4.

Equation 5.22a enables the calculation of the chemical potential of water in the hydrate as a function of the fractional occupation in the cavities. Equation 5.18 provides the chemical potential of water in terms of the chemical potential in the empty hydrate, as well as the product of the individual cavity partition function and the absolute activity:

$$\frac{\mu_w^H}{kT} = \frac{\mu_w^\beta}{kT} - \sum_i v_i \ell \ln \left( 1 + \sum_J q_{J,i} \lambda_J \right) \quad (5.18)$$

Since the final product is  $q_{J,i} \lambda_J = C_{J,i} P_J$  by Equation 5.21 then

$$\frac{\mu_w^H}{kT} = \frac{\mu_w^\beta}{kT} - \sum_i v_i \ell \ln \left( 1 + \sum_J C_{J,i} P_J \right) \quad (5.18a)$$

Now consider the logarithmic term in Equation 5.18a. It may be simplified through the use of Equation 5.22a, which relates  $\theta_{J,i}$ , the fractional occupation of a cavity of type  $i$  by a molecule of type  $J$ , to the Langmuir constant

$$\ell \ln \left( 1 - \sum_J \theta_{J,i} \right) = \ell \ln \left( 1 - \sum_J \frac{C_{J,i} P_J}{1 + \sum_J C_{J,i} P_J} \right)$$

or

$$\ell n \left( 1 - \sum_J \theta_{J,i} \right) = \ell n \left( \frac{1}{1 + \sum_J C_{J,i} P_J} \right) = - \ln \left( 1 + \sum_J C_{J,i} P_J \right)$$

Substitution of the above equation into Equation 5.18a yields:

$$\mu_W^H = \mu_W^\beta + kT \sum_i v_i \ell n \left( 1 - \sum_J \theta_{J,i} \right) \quad (5.23)$$

Equation 5.23 may be used with Equation 5.22a to determine the chemical potential of water in hydrate  $\mu_W^H$ , which is one of the major contributions of the model. The combination of these two equations is of vital importance to phase equilibrium calculations, since the method equates the chemical potential of a component in different phases, at constant temperature and pressure.

Equation 5.23 shows that an increased filling of the cavities causes a decrease in the value of  $\mu_W^H$  so that the hydrate becomes more thermodynamically stable. In the large cavities particularly, the fractional occupation  $\theta_{J,i}$  frequently approaches unity, causing the water chemical potential to be substantially lowered because the logarithm of a small fraction  $(1 - \sum \theta_{J,i})$  is a large negative number.

At the other occupation extreme, if the value of  $\theta_{J,i}$  were unrealistically small in Equation 5.23, the final term could be replaced by  $-kT \sum_i \sum_J v_i \theta_{J,i}$ . The resulting equation is van't Hoff's law:

$$\mu_W^H = \mu_W^\beta - kT \sum_i \sum_J v_i \theta_{J,i} \quad (5.23a)$$

which is used in other applications to model ideal, dilute, solid solutions (Lewis and Randall, 1923, p. 238). Thus the above limiting forms of Equation 5.23 lends mathematical credence to the hydrate solid solution concept, which is the basis of the current model as well as the Katz distribution coefficient ( $K_{vs_i}$ ) method of Section 4.2.2. Equations 5.23 and 5.23a also show that hydrates are stabilized by an increase in the cavity occupation,  $\theta_{k_i}$ , which lowers the chemical potential of water.

### Example 5.1: Determination of Hydrate Nonstoichiometry

Cady (1983a,b) provided the below illustration of how Equations 5.22a and 5.23 may be used to determine the hydration number for seven simple hydrates of structure I.

From Chapter 2, recall that structure I has 46 water molecules in the basic crystal with 6 large ( $5^{12}6^2$ ) cavities and 2 small ( $5^{12}$ ) cavities. For ideal

sI hydrates, if all of the cavities were filled the hydration number (water molecules per guest molecule) would be  $n = 46/8$ . For simple hydrates, the hydration number is related to the fractional filling of the large and small cavities,  $\theta_L$ , and  $\theta_S$ , respectively as

$$n = \frac{46}{6\theta_L + 2\theta_S} = \frac{23}{3\theta_L + \theta_S} \quad (\text{E5.1.1})$$

Equation 5.22a applied to each size cavity gives

$$\theta_L = \frac{C_L P}{1 + C_L P} \quad (\text{E5.1.2a})$$

and

$$\theta_S = \frac{C_S P}{1 + C_S P} \quad (\text{E5.1.2b})$$

Now if the formation pressure is considered for a simple hydrate at 273.15 K, we may obtain from Equation 5.23 with Davidson's (1973) suggestion that  $\mu_W^H - \mu_W^\beta = -1108 \text{ J/gmol}$ .

$$-0.4885 = \frac{3}{23} \ln(1 - \theta_L) + \frac{1}{23} \ln(1 - \theta_S) \quad (\text{E5.1.3})$$

Cady suggested that a value of  $n$  may be estimated at a pressure corresponding to 273.15 K for a hydrated guest using de Forcrand's method with the Clapeyron equation (Section 4.6.2.1). Equations E5.1.1 and E5.1.3 may then be solved simultaneously for  $\theta_L$  and  $\theta_S$ . In turn,  $\theta_L$  and  $\theta_S$  may be substituted into Equation E5.1.2a and b to calculate  $C_L$  and  $C_S$ . Since the values of  $C_L$  and  $C_S$  are constant at constant temperature, they may be used to determine the hydrate numbers at pressures higher than the equilibrium value, using Equations E5.1.1 and E5.1.2.

Using the above method, Cady compared the calculated hydrate numbers to his experimental values, with results as shown in [Figure 5.1](#). The fit of the equations to the experiment seems to be remarkably good.

### Example 5.2: Calculation of Hydrate Density

With values for the fractional filling of each cavity type, hydrate density may be determined based upon a unit crystal. Additional required input data are the dimensions of a unit crystal, the number of water molecules per crystal and the number of small and large cavities per unit crystal, as specified in [Table 2.2](#). Based upon a single unit cavity, the hydrate density ( $\rho$ ) may be calculated by the formula:

$$\rho = \frac{N_w \text{MW}_{\text{H}_2\text{O}} + \sum_{J=1}^C \sum_{i=1}^N \theta_{iJ} v_i \text{MW}_J}{N_{\text{Ava}} V_{\text{cell}}} \quad (\text{E5.2.1})$$

where

$N_w$  = number of water molecules per unit cell ([Table 2.2](#))

$N_{\text{Av}}$  = Avagadro's number,  $6.023 \times 10^{23}$  molecules/mol

$\text{MW}_J$  = molecular weight of component  $J$

$\theta_{iJ}$  = fractional occupation of cavity  $i$  by component  $J$  (computer program)

$v_i$  = number of type  $i$  cavities per water molecule in unit cell ([Table 2.2](#))

$V_{\text{cell}}$  = volume of unit cell (dimensions in [Table 2.2](#))

$N$  = number of cavity types in unit cell

$C$  = number of components in hydrate phase

**Example 5.2a:** Calculate the density of methane hydrate at 273.15 K

*Solution*

From the computer program included with this book, at 273.15 K the hydrate is predicted to have a dissociation pressure of 25.1 atm. The hydrate is predicted to be sI, with a fractional occupancy of cavities as  $\theta_s = 0.870$  and  $\theta_L = 0.973$ . There are 46 water molecules per sI unit cell, with 2 small ( $5^{12}$ ) and 6 large ( $5^{12}6^2$ ) cavities, and the unit cell length is 12 Å on one side. The density is then calculated from [Equation E5.2.1](#) as

$$\rho = \frac{(46 \times 18) + [(0.87 \times 2 \times 16) + (0.973 \times 6 \times 16)]}{(6.023 \times 10^{23}) \times (12.0)^3 \times (10^{-8})^3} = 0.91 \text{ g/cc}$$
(E5.2.2)

The above density can be compared to that calculated by Makogon (1974, p. 31) as 0.897 g/cc.

**Example 5.2b:** Calculate the hydrate density resulting from a gas mixture (90 mol% CH<sub>4</sub>, 7% C<sub>2</sub>H<sub>6</sub>, 3% C<sub>3</sub>H<sub>8</sub>) at 277 K

*Solution*

From the computer program included with this book, at 277 K the hydrate is predicted to be sII with a dissociation pressure of 12.9 atm. The length of one side of sII is 17.3 Å, with 136 water molecules, as well as 16 small ( $5^{12}$ ) and 8 large ( $5^{12}6^4$ ) cavities per unit cell. The fractional filling of each cavity ( $\theta_i$ ) is given in the below table:

	CH <sub>4</sub>	C <sub>2</sub> H <sub>6</sub>	C <sub>3</sub> H <sub>8</sub>
$\theta_s$	0.67	0	0
$\theta_L$	0.057	0.096	0.84
MW	16	30	44

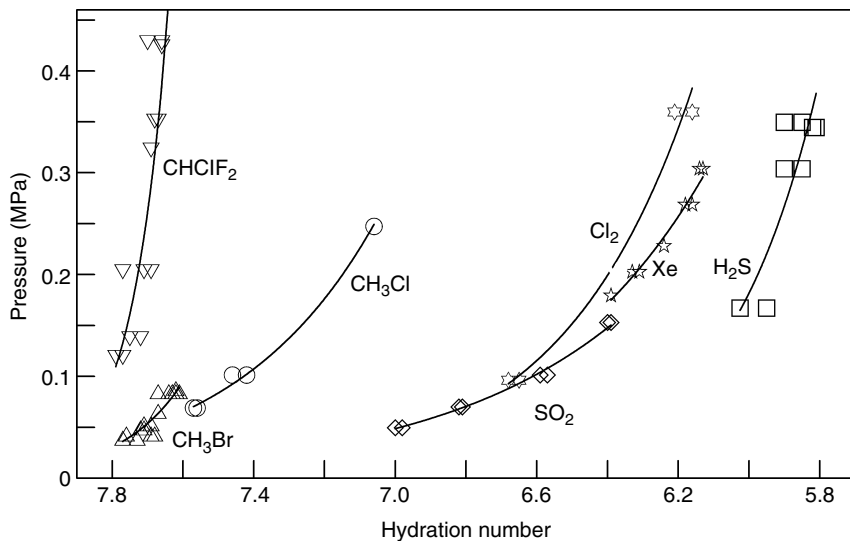


**FIGURE 5.1** Change of hydration number with pressure. (Reproduced from Cady, G.H., *J. Phys. Chem.*, **85**, 4437 (1983a). With permission from the American Chemical Society.)

Using Equation E5.2.1 the density is computed as

$$\begin{aligned}\rho = & [(136 \times 18) + [(0.67 \times 16 \times 16) + (0.057 \times 8 \times 16)] \\ & + [0.096 \times 8 \times 30] + [0.84 \times 8 \times 44]] \\ & \times [(6.023 \times 10^{23}) \times (17.3)^3 \times (10^{-8})^3]^{-1} = 0.94 \text{ g/cc} \quad (\text{E5.2.3})\end{aligned}$$

There are no measurements or calculations of this quantity for comparison.

### 5.1.3 The Langmuir Adsorption Analogy

In single component Langmuir adsorption, one finds many analogies to the process of guest encapsulation in the hydrate cavity, to provide a physical interpretation of guest containment. In the below listing of single component Langmuir adsorption isotherm assumptions, the analogies are readily apparent through a replacement of the words “adsorption or desorption” with “enclathration or declathration,” the word “sites” should be replaced by “cavities,” and the word “surface” should be replaced by “crystal unit cell.” The assumptions are

1. The adsorption of gas molecules occurs at discrete sites on the surface.
2. The energy of adsorption on the surface is independent of the presence of other adsorbed molecules.

3. The maximum amount of adsorption corresponds to one molecule per site.
4. The adsorption is localized and occurs by collision of gas phase molecules with vacant sites.
5. The desorption rate depends only on the amount of adsorbed material on the surface.

To illustrate the analogy more clearly, it is necessary to consider the derivation of the Langmuir adsorption isotherm. We can incorporate the above assumptions into an equilibrium expression which equates the rate of adsorption  $r_{\text{ads}}$  to that of desorption  $r_{\text{des}}$  of gas molecules of type  $J$ . The desorption rate is directly proportional to the fraction of monolayer sites occupied  $\Theta_J$ , and is expressed as

$$r_{\text{des}} = \chi' \Theta_J$$

where  $\chi'$  is taken as the proportionality constant (sometimes called the desorption rate constant), which is only a function of temperature. The rate of adsorption is proportional to the product of the gas pressure  $P_k$  and the number of unoccupied sites  $(1 - \Theta_J)$  in the equation

$$r_{\text{ads}} = \chi P_J (1 - \Theta_J)$$

At equilibrium, the above rates of adsorption and desorption are equated, and an expression is obtained for the fraction of sites occupied  $\Theta_J$ , which appears identical to Equation 5.22a for simple hydrates of one component:

$$\Theta_J = \frac{\chi P_J}{\chi' + \chi P_J} = \frac{KP_J}{1 + KP_J} \quad (5.22b)$$

where the equilibrium Langmuir adsorption constant ( $K \equiv \chi/\chi'$ ) is analogous to the Langmuir hydrate constant  $C_{Ji}$  in Equation 5.22a; both are only functions of temperature and the components (adsorbed species and site or specific cavity). One difference is that the Langmuir constant in hydrates provides for more than one type of cavity (analogous to another type of adsorption site) with the additional subscript “ $i$ .”

Consider the physical meaning of the terms in the simple hydrate analog (Equation 5.22a) of the Langmuir Equation 5.22b above, with the pressure corrected as fugacity:

$$\theta_{J,i} = \frac{C_{J,i} f_J}{1 + C_{J,i} f_J} \quad (5.22c)$$

The fraction of the adsorbed monolayer  $\Theta_J$  in (Equation 5.22b) is analogous to the fractional occupation of the cavities of type  $i$ ,  $\theta_{J,i}$  (Equation 5.22a). The fractional occupation of each cavity will increase as the product  $(C_{J,i} f_J)$  increases. In the limit, for very large values of  $C_{J,i} f_J$  the fractional occupancy approaches unity.

In other words,  $C_{Ji}$  measures the “attractiveness” of the cage for a hydrated species. At a given value of fugacity, the most strongly enclathrated component in a cavity is the component with the highest values of  $C_{Ji}$ . In Section 2.1.3.2 it was suggested that there was an optimal fit of the guest molecule within a host cavity; this optimal fit provides a higher value of the Langmuir constant.

For example, a very small molecule in a large ( $5^{12}6^4$ ) cavity has a smaller Langmuir constant than the same molecule within a  $5^{12}$  cavity as first shown by Holder and Manganiello (1982). In contrast, the Langmuir constant would be zero for a molecule slightly too large to fit the small cavity, but the Langmuir constant would be substantial for the same molecule within the large cavity.

Similarly, at a given value of the Langmuir constant, higher values of fugacity provide for higher fractional filling of each cavity. Loosely, fugacity may be physically interpreted as “thermodynamically corrected” pressure. Thus higher pressures provide higher fractional filling of each cavity.

However, it should be remembered that the fractional filling is a function of the product  $C_{Ji}f_i$ , rather than either factor in the product. Finally, in the original van der Waals and Platteeuw approach the Langmuir constants for both adsorption and enclathration were only functions of temperature for each molecule type retained at the individual site or cavity. In the modified approach below, the Langmuir constants are also a function of cage size, or the unit cell volume, which is a function of the hydrate guests, temperature, and pressure.

### 5.1.4 Relating the Langmuir Constant to Cell Potential Parameters

With the adsorption analogy in mind, the next object is to relate the Langmuir constants  $C_{J,i}$  to experimental variables, by providing a physical interpretation. In order to consider the Langmuir constant, it is first necessary to determine the individual guest potential energy within the cavity. The force between the guest and cavity is the change in the potential energy with the guest displacement. We must first make two assumptions, in addition to the four assumptions made for the hydrate in Section 5.1.1:

1. The internal motion partition function of the guest molecule is the same as that of an ideal gas. That is, the rotational, vibrational, nuclear, and electronic energies are not significantly affected by enclathration, as supported by spectroscopic results summarized by Davidson (1971) and Davidson and Ripmeester (1984).
2. The potential energy of a guest molecule at a distance  $r$  from the cavity center is given by the spherically symmetrical potential  $\varpi(r)$  proposed by Lennard-Jones and Devonshire (1932, 1938).

Assumptions (1) and (2) above are more restrictive than assumptions (1) through (4) in Section 5.1.1, in that they apply more to monatomic or spherical

molecules than for oblate or polar molecules. Prediction inaccuracies of the model for certain gases may be related to errors in these assumptions.

In this model the interactions of the guest with the nearest neighboring  $z_i$  water molecules of a spherical cage are summed in a pair-wise manner. The model obtains a function  $\varpi(r)$  describing the resulting field, averaged over all positions of the molecules within the cavity. The fundamental intermolecular potential between a water molecule of the cavity wall and a solute molecule may be described by a number of intermolecular potentials.

The original work by van de Waals and Platteeuw (1959) used the Lennard-Jones 6–12 pair potential. McKoy and Sinanoglu (1963) suggested that the Kihara (1951) core potential was better for both larger and nonspherical molecules. The Kihara potential is the potential currently used, with parameters fitted to experimental hydrate dissociation data. However, it should be noted that the equations presented below are for a spherical core, and while nonspherical core work is possible, it has not been done for hydrates.

The pair potential energy  $\Phi$  between the guest molecule and any water molecule is related to the force ( $F$ ) each exerts on the other by,  $F = -\partial\phi/\partial r$  where “ $r$ ” is the molecular center distance between the two. The potential, which itself is a function of separation distance, is unique to every molecular type and is given by

$$\Phi(r) = \infty \quad \text{for } r \leq (a_g + a_w) \quad (5.24a)$$

$$\Phi(r) = 4\varepsilon \left\{ \left( \frac{\sigma}{r - 2a} \right)^{12} - \left( \frac{\sigma}{r - 2a} \right)^6 \right\} \quad \text{for } r > (a_g + a_w) \quad (5.24b)$$

where

$\sigma$  = cores distance at zero potential ( $\Phi = 0$ ), (attraction and repulsion balance),

$a$  = radius of the spherical core ( $g$  = guest and  $w$  = water) and

$\varepsilon$  = maximum attractive potential (at  $r = \sqrt[6]{2}\sigma$ ).

The Lennard-Jones–Devonshire theory (as summarized by Fowler and Guggenheim, 1952, pp. 336ff) averaged the pair potentials of Equation 5.24a and b between the solute and each water, for  $z_i$  molecules in the surface of the spherical cavity to obtain a cell potential  $\varpi(r)$  of

$$\varpi(r) = 2z\varepsilon \left[ \frac{\sigma^{12}}{R^{11}r} \left( \delta^{10} + \frac{a}{R} \delta^{11} \right) - \frac{\sigma^6}{R^5r} \left( \delta^4 + \frac{a}{R} \delta^5 \right) \right] \quad (5.25a)$$

where

$$\delta^N = \frac{1}{N} \left[ \left( 1 - \frac{r}{R} - \frac{a}{R} \right)^{-N} - \left( 1 + \frac{r}{R} - \frac{a}{R} \right)^{-N} \right] \quad (5.25b)$$

where

$N = 4, 5, 10,$  or  $11$ , indicated in Equation 5.25a,

$z$  = the coordination number (number of water molecules) of the cavity,

$R$  = the free cavity radius,<sup>1</sup> (assuming “smeared” spherical cavity), and

$r$  = distance of the guest molecule from the cavity center.

The spherical averaging of the potential function over all the angles of interaction with the wall enables the potential of Equation 5.25a and b) to be expressed solely in terms of distance  $r$  from the cavity center for a given guest molecule. It should be noted that the parameters  $\varepsilon$ ,  $a$ , and  $\sigma$  are unique for every guest molecule, but they do not change in the different cavity types. On the other hand, the parameters  $z$  and  $R$  have been uniquely determined for each type cavity by x-ray diffraction data (see Table 2.1) and do not change as a function of guest molecules.

Following van der Waals and Platteeuw (1959, pp. 26ff) the individual particle partition function is related to the product of three factors: (1) the cube of the de Broglie wavelength, (2) the internal partition function, and (3) the configurational triple integral, as

$$q_{Ji} = \left( \frac{2\pi mkT}{h^2} \right)^{3/2} q_{\text{int}} \int_0^{2\pi} \int_0^\pi \int_0^R \exp \left( -\frac{\varpi(r)}{kT} \right) r^2 \sin \theta \, dr \, d\theta \, d\phi \quad (5.26)$$

The cavities are assumed to be spherically symmetric, which enables the elimination of the two angular portions of the triple integral, resulting in  $4\pi$ . Substitution of the resulting equation into Equation 5.21 yields the final expression for the Langmuir constant in terms of the particle potential within the cavity.

$$C_{J,i} = \frac{4\pi}{kT} \int_0^R \exp \left( -\frac{\varpi(r)}{kT} \right) r^2 \, dr \quad (5.27a)$$

The evaluation of the Langmuir constant may then be determined from a minimum of experimentally fitted Kihara parameters via an integration over the cavity radius. Equation 5.27a shows the Langmuir constant to be only a function of temperature for a given component within a given cavity.

The experimentally fitted hydrate guest Kihara parameters in the cavity potential  $\varpi(r)$  of Equation 5.25 are not the same as those found from second virial coefficients or viscosity data for several reasons, two of which are listed here. First, the Kihara potential itself does not adequately fit pure water virials over a wide range of temperature and pressure, and thus will not be adequate for water–hydrocarbon mixtures. Second, with the spherical Lennard-Jones–Devonshire theory the point-wise potential of water molecules is “smeared” to yield an averaged spherical shell potential, which causes the water parameters to become indistinct. As a result, the Kihara parameters for the guest within the cavity are fitted to hydrate formation properties for each component.

---

<sup>1</sup> Values given in Table 2.1, minus 1.45 Å for the free cavity radius of water to obtain  $R$ .

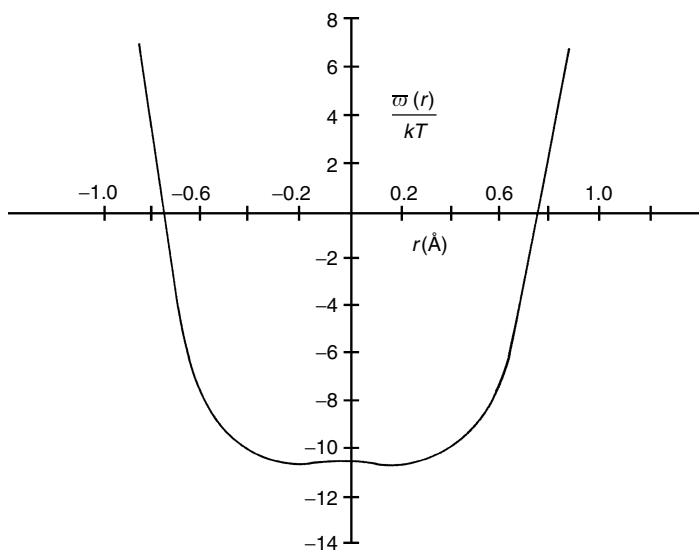


**FIGURE 5.2** Typical spherically symmetrical cavity potential function between guest and cell. (Reproduced from McKoy, V., Sinanoglu, O., *J. Chem. Phys.*, **38**, 2946 (1963). With permission from the American Institute of Physics.)

A typical potential  $\varpi(r)$  is shown in Figure 5.2. Note that the potential is more negative (high attraction) in the center of the cell, or at some distance from the cell wall, with high repulsion (positive values) at the cell wall. As the guest molecule approaches one wall of the cavity, it is both repulsed by that wall and attracted by the opposite wall, causing it to exist in the center. Recent work in molecular simulation suggests that smaller molecules are located in local minima away from the center, and that the repulsive portion of the potential is more important than the attraction (see the molecular simulation discussion in Section 5.3).

Equation 5.27a shows that the main contribution to the Langmuir constant comes from integrating the guest–cavity pair potential in the interior of the cells. This is a partial explanation of the reason why the final assumption (2) at the beginning of this subsection for “smeared water molecules” is a good approximation for the cavity shell; in addition the cavities are spherical, to a first approximation.

The value of fitting the Langmuir constants to simple hydrate formation data is in the prediction of mixture hydrate formation. When the formation data for the simple hydrates are adequately fitted, then mixtures of those guest components can be predicted with no adjustable parameters. Since there are only eight simple hydrate formers of natural gas which form sI and sII, but an infinite variety of mixtures, such an advantage represents a substantial savings of time and effort.

In the development of Equation 5.27a, it was assumed that the interaction between the guest and the water molecules in cage  $m$  could be approximated using an average cage radius. Ballard (2002) suggested another approach. He proposed

**TABLE 5.2****Types of Oxygen Atoms at the Periphery of Both SI and SII Hydrate Cages and Distance of Each to the Center of the Cages**

	Small cage ( $5^{12}$ )			Large cage ( $5^{12}6^4$ )		
(a) sI ethylene oxide hydrate ( $a = 12.03 \text{ \AA}$ ) (McMullan and Jeffrey, 1965)						
No. of water molecules in cage	20			24		
Average radius ( $\text{\AA}$ )	3.908			4.326		
Layer type	(i)	(k)		(i)	(k)	(c)
No. of water molecules in layer	8	12		8	8	4
Radius ( $\text{\AA}$ )	3.83	3.96		4.47	4.06	4.645
						4.25
	Small cage ( $5^{12}$ )			Large cage ( $5^{12}6^4$ )		
(b) sII tetrahydrofuran and hydrogen sulfide hydrate ( $a = 17.1 \text{ \AA}$ ) (Mak and McMullan, 1965)						
No. of water molecules in cage	20			28		
Average radius ( $\text{\AA}$ )	3.902			4.683		
Layer type	(a)	(e)	(g)		(e)	(g)
No. of water molecules in layer	2	6	12		4	12
Radius ( $\text{\AA}$ )	3.748	3.845	3.956		4.729	4.715
						4.635

that the interactions between the guest and water molecules can be better approximated using a “multilayered” cage, using direct single crystal diffraction data for the radii of each water molecule in the hydrate cages (Mak and McMullan, 1965; McMullan and Jeffrey, 1965). Table 5.2 lists these radii for sI and sII hydrates. Note that the cubic lattice parameter, which corresponds to these cage radii, is given for each hydrate structure. Equation 5.27b is the proposed expression for the Langmuir constant:

$$C_{J,m} = \frac{4\pi}{kT} \int_0^{R_1 - aj} \exp \left[ -\frac{\sum_n \omega_{J,n}(r)}{kT} \right] r^2 dr \quad (5.27b)$$

where the summation is over all shells ( $n$ ) in cage  $m$ , and  $aj$  is the hard core radius, subtracted from  $R$  to avoid singularities. Note that the upper limit of the integral is evaluated at  $R_1$ , which is the smallest shell in cage  $m$ . Equation 5.27a can still be used to evaluate the potential for a given layer. In the development of Equation 5.27b, it was assumed that binary interactions between the guest and the water molecules (shells) are of most importance.

The crucial change introduced in CSMGem is to make the radii of each shell functions of temperature, pressure, and composition. As the lattice expands or compresses, the cages also expand or compress. The radii of the shells are assumed to be a linear function of the cubic hydrate lattice parameter. For example, if the lattice parameter expands by 1% of its original value, each shell radius,  $R_n$ , also expands by 1% of its original value. In addition the concept of various distances from the average are included to separate a single cavity into oxygens that are

**TABLE 5.3**  
**Summary of the Equations for Fitting Simple Hydrate Formers**

$$\theta_{k_i} = \frac{C_{k_i} f_k}{1 + \sum_j C_{j_i} f_j} \quad (5.22c)$$

$$\mu_w^H = g_w^\beta + RT \sum_i v_i \ln \left( 1 - \sum_j \theta_{iJ} \right) + RT \ln \gamma_w^H \quad (5.28)$$

$$\varpi(r) = 2z\varepsilon \left[ \frac{\sigma^{12}}{R^{11}r} \left( \delta^{10} + \frac{a}{R} \delta^{11} \right) - \frac{\sigma^6}{R^5r} \left( \delta^4 + \frac{a}{R} \delta^5 \right) \right] \quad (5.25a)$$

$$\text{where } \delta^N = \frac{1}{N} \left[ \left( 1 - \frac{r}{R} - \frac{a}{R} \right)^{-N} - \left( 1 + \frac{r}{R} - \frac{a}{R} \right)^{-N} \right] \quad (5.25b)$$

$$C_{J,m} = \frac{4\pi}{kT} \int_0^{R_1-a_J} \exp \left[ - \frac{\sum_n \omega_{J,n}(r)}{kT} \right] r^2 dr \quad (5.27b)$$

closer (or further) from the center, and sums the interaction energies over those coordination numbers.

It should be noted here that Bazant and Trout (2001) developed an ingenious mathematical method to determine the Langmuir constant for guest molecules which only fill the large cage, relating them to the calculated fluid phase fugacity and the experimentally determined change in chemical potentials in Equation 5.23, via the relations:

$$\text{For structure I large guests } C_{J,i} = \frac{\exp(23/3 \Delta \mu_w^{\beta-H}/kT) - 1}{f_J} \quad (5.27c)$$

$$\text{For structure I large guests } C_{J,i} = \frac{\exp(17/1 \Delta \mu_w^{\beta-H}/kT) - 1}{f_J} \quad (5.27d)$$

Using the above equations, the Langmuir constant for the large cavity occupant can be determined explicitly from the chemical potential difference and the fugacity. However, for systems in which both cavities are occupied, a second method must be used to supplement Equation 5.27c and d.

Table 5.3 summarizes the previous equations for simple hydrate formers.

### 5.1.5 Activity Coefficient for Water in the Hydrate

Several methods have arisen to correct the assumptions in the above van der Waals and Platteeuw model, to address the inaccuracies at the high pressures of current applications. The two most prominent modern correction methods are: (1) to use *ab initio* quantum mechanical corrections to relate to first principles as much possible, as briefly discussed in Section 5.1.9, and (2) to fit the existing

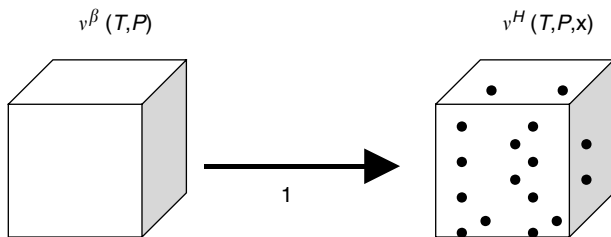


**FIGURE 5.3** Filling the empty cages without distortion. Van der Waals and Platteeuw model without distortion of hydrate due to guests ( $v^B = v^H$ ). Process (1) in Figure 5.3 is given by the summation term in Equation 5.23.

macroscopic (phase equilibria) and microscopic (spectroscopic) data as physically and as accurately as possible to a modified van der Waals and Platteeuw theory.

Because there is a very large phase equilibrium data base, existing over 70 years as shown in Chapter 6, and because recent spectroscopic tools (e.g., Raman, NMR, and diffraction) have provided microscopic hydrate data, the latter approach was chosen in this monograph and the accompanying computer programs. While the latter method used in this book represents a theoretical advance, it is shown to compare favorably with the existing commercial hydrate programs in Section 5.1.8.

In particular, the extension of the van der Waals and Platteeuw method addresses the first assumption listed at the beginning of Section 5.1.1—namely that encaged molecules do not distort the cavity. In the development of the statistical thermodynamic hydrate model (Equation 5.23), the free energy of water in the standard hydrate (empty hydrate lattice),  $g_w^\beta$ , is assumed to be known at a given temperature ( $T$ ) and volume ( $v$ ). Since the model was developed at constant volume, the assumption requires that the volume of the empty hydrate lattice,  $v^\beta$ , be equal to the volume of the equilibrium hydrate,  $v^H$ , so that the only energy change is due to occupation of the hydrate cavities, as shown in Figure 5.3.

Traditionally, the chemical potential of the standard hydrate is assumed to be at a given volume, independent of the hydrate guests. If the standard hydrate volume is not the volume of the equilibrium hydrate, there should be an energy change proportional to the difference in volume ( $\Delta v^H = v^H - v^\beta$ ). Note that, in the development of Equation 5.23,  $\Delta v^H$  is assumed to be equal to zero (i.e., all hydrates of a given structure are at the same volume).

Equation 5.23 is considered to be an ideal solid solution model. If we choose to extend our equations from one hydrate crystal to a large number  $N_A$  (Avogadro's number) of crystals, we must replace the Boltzmann constant "k" with the universal gas constant  $R$  ( $\equiv kN_A$ ). Ballard (2002) defined the chemical potential of water in hydrates as

$$\mu_w^H = g_w^\beta + RT \sum_i v_i \ln \left( 1 - \sum_j \theta_{ij} \right) + RT \ln \gamma_w^H \quad (5.28)$$

noting that the empty water chemical potential equals that of the Gibbs energy, and where the activity coefficient of water in the hydrate,  $\gamma_w^H$ , accounts for nonidealities due to the inclusion of the hydrate guests, which enlarge the hydrate cavities. Diffraction data show that the volume of the hydrate is a strong function of the guest(s) present in the hydrate (von Stackelberg and Jahns, 1954; Huo, 2002). Therefore, Ballard suggested that the activity coefficient be a function of the difference in volume between the hydrate and the standard hydrate,  $\Delta v^H$ , noting that the activity coefficient has the following property:

$$\gamma_w^H \rightarrow 1 \quad \text{as } \Delta v^H \rightarrow 0 \text{ or as } x_w^H \rightarrow 1$$

At the limit stated above, Equation 5.28 reduces to Equation 5.23 when  $\Delta v^H = 0$  (i.e.,  $\gamma_w^H = 1$ ). In the strictest sense, the activity coefficient accounts for the energy change involved in taking the volume of the standard lattice to the volume of the real hydrate. That is, it will perturb the Gibbs energy of the standard lattice such as

$$\mu_w^H = g_w^\beta + \Delta g_w^\beta + RT \sum_i v_i \ln \left( 1 - \sum_J \theta_{iJ} \right) \quad (5.29)$$

where the perturbation can be described as

$$\Delta g_w^\beta = \frac{\Delta g_{w0}^\beta}{RT_0} - \int_{T_0}^T \frac{\Delta h_w^\beta}{RT^2} dT + \int_{P_0}^P \frac{\Delta v^H}{RT} dP \quad (5.30)$$

Evaluating Equations 5.28 through 5.30, and assuming that the heat capacity of the hydrate is not affected in the process, Ballard proposed that the activity coefficient of water in the hydrate be expressed as

$$\ln \gamma_w^H = \frac{\Delta g_{w0}^\beta}{RT_0} + \frac{\Delta h_{w0}^\beta}{R} \left( \frac{1}{T} - \frac{1}{T_0} \right) + \int_{P_0}^P \frac{\Delta v^H}{RT} dP \quad (5.31)$$

where  $h_{w0}^\beta$  is the enthalpy of formation at reference conditions. Ballard (2002) arbitrarily defined the perturbed Gibbs energy and enthalpy of formation be linear in  $\Delta v^H$ ;  $\Delta g_{w0}^\beta = a\Delta v_0^H$ , and  $\Delta h_{w0}^\beta = b\Delta v_0^H$ . Note that the subscript 0 refers to the volume difference at  $T_0$  and  $P_0$ , the temperature and pressure at which the formation properties are known. This definition satisfies the above constraint on the activity coefficient—namely that it should approach unity in the limit of a pure water (hypothetical) hydrates.

[Figure 5.4](#) illustrates the processes needed to determine the chemical potential of water in the hydrate, as given by Equation 5.28

$$g_w^\beta + RT \sum_i v_i \ln \left( 1 - \sum_J \theta_{iJ} \right) + RT\gamma_w^H = \mu_w^H$$

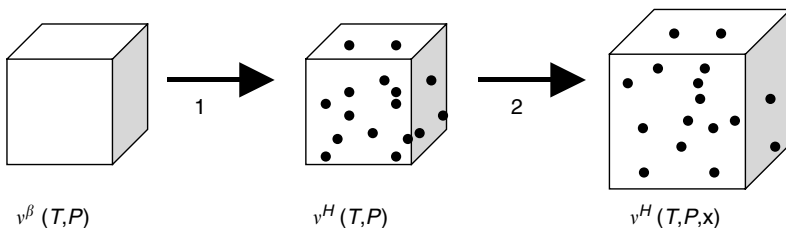


**FIGURE 5.4** Corrected model allowing for distortion of hydrate due to guests ( $v^\beta \neq v^H$ ). Process (1) in Figure 5.4 is done at constant volume and therefore, the van der Waals and Platteeuw statistical model can be used. Process (2) in Figure 5.4, the volume change of the hydrate from its standard state volume, is done at constant composition and is described by the activity coefficient in Equation 5.28.

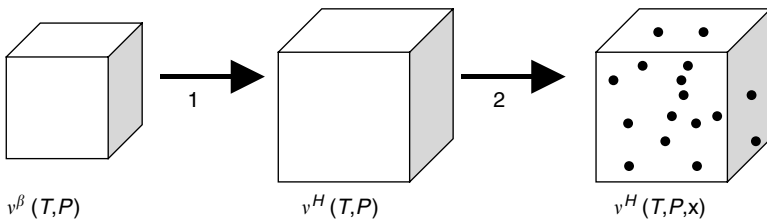


**FIGURE 5.5** Alternative expression for corrected model allowing for distortion of hydrate ( $v^\beta \neq v^H$ ). Equation 5.29 is the analogous expression for the processes shown.

Ballard (2002) noted that chemical potential is a state function and, therefore Equation 5.28 can be visualized in another path (as shown in Figure 5.5).

$$g_w^\beta + \Delta g_w^\beta + RT \sum_i v_i \ln \left( 1 - \sum_j \theta_{ij} \right) = \mu_w^H$$

In Figure 5.5, process (1) is given by Equations 5.30 and 5.31 and process (2) by the van der Waals and Platteeuw statistical model, since it is done at constant volume. Note that, since chemical potential is a state function, Figures 5.4 and 5.5 are equivalent processes.

The reader may be confused by the suggestion that the empty hydrate lattice being distorted by the addition of guests. Yet the method is pragmatically justified because it would be impossible to measure the empty lattice energies for all possible combinations of hydrate components. So we simply use methane for sI (or propane for sII, or methane + neohexane for sH) as a reference case. With these references, the deviation occurs because an empty methane lattice is not the same as an empty CO<sub>2</sub> or xenon lattice, and thus we try to account for that by using this activity term. This point is further discussed in Section 5.1.6.

### 5.1.6 Defining the Hydrate Fugacity and Reference Parameters

Ballard (2002) defined a hydrate fugacity with three major advantages:

1. The aqueous phase does not need to be present to enable hydrate calculations. Frequently, gas or condensate pipelines have no aqueous phase.
2. The properties of the empty hydrate are directly used in the model as opposed to the difference properties suggested by Parrish and Prausnitz (1972).
3. The expression for the fugacity of water in the hydrate follows the same framework as that in all other phases (i.e., aqueous, vapor or liquid, or pure solid phases).

In order to solve for thermodynamic equilibrium, the fugacity of water in the hydrate must be known. This method follows the common approach of solving for fugacity, using the standard state of the ideal gas of the pure component at 1 bar.

$$f_w^H = f_{w,o} \exp \left[ \frac{\mu_{w,H}^H - g_{w,o}}{RT} \right] \quad (5.32)$$

where  $f_{w,o}$  is 1 bar,  $g_{w,o}$  is the Gibbs energy of pure water in the ideal gas state at 1 bar, and  $\mu_{w,H}$  is given by Equation 5.28. Note that the fugacity of water in the hydrate, as determined by Equation 5.32, does not require that an aqueous phase be present.

The best choice for the standard hydrate is one that is well-characterized and not too different from the real state of the system. If the standard state is well-defined, small perturbations from this standard state can be accounted for correctly. With this in mind, we turn to the three most well-known hydrates of sI, sII, and sH, namely methane, propane, and methane + neohexane. Note that the standard states for sI, sII, and sH are the empty hydrate lattices of these and not the actual hydrates. Therefore for the reference hydrates, the activity coefficients for methane, propane, and methane + neohexane hydrates will be unity.

The Gibbs energy of water in the standard state can be corrected for temperature and pressure using classical thermodynamics.

$$\frac{g_w^\beta}{RT} = \frac{g_{w_0}^\beta}{RT_0} - \int_{T_0}^T \frac{h_w^\beta}{RT^2} dT + \int_{P_0}^P \frac{v_w^\beta}{RT} dP \quad (5.33)$$

Note that  $g_{w_0}^\beta$  is the molar Gibbs energy of formation of the standard hydrate at the reference conditions ( $T_0$  and  $P_0$ ),  $h_w^\beta$  is the molar enthalpy, and  $v_w^\beta$  is the molar

volume. These three properties are the unknowns which should be determined in order to specify the standard state hydrate.

The molar enthalpy of water in the standard hydrate can be expressed as

$$h_w^\beta = h_{w0}^\beta + \int_{T_0}^T c_{P_w^\beta} dT \quad (5.34)$$

where  $h_{w0}^\beta$  is the molar enthalpy of formation of the standard hydrate at the reference conditions ( $T_0$  and  $P_0$ ) and  $c_{P_w^\beta}$  is the heat capacity. The heat capacity of the standard hydrates for both sI and sII is well approximated by that of ice (Avlonitis, 1994), as is that for sH. However, the molar enthalpy of formation is not known and must be regressed to experimental data.

We define the molar volume of the standard hydrates of sI and sII as the molar volumes of methane and propane hydrate, respectively. The molar volume of these hydrates, and therefore of the standard states, is well-characterized via diffraction data (Tse, 1990; Huo, 2002). Ballard proposed the following expression for the molar volume of water in hydrates:

$$v_w^\beta = v_0 \exp[\alpha_1(T - T_0) + \alpha_2(T - T_0)^2 + \alpha_3(T - T_0)^3 - \kappa(P - P_0)] \quad (5.35)$$

The compressibility coefficient,  $\kappa$ , and reference volume,  $v_0$ , are solely dependent on the composition of the guest(s) in the hydrate lattice while the thermal expansion coefficients,  $\alpha_1$ ,  $\alpha_2$ , and  $\alpha_3$  are solely dependent on the hydrate structure.

Note that, since all hydrates of a given structure have the same thermal expansion, the values in Table 5.4 are also the thermal expansion parameters for the standard empty hydrates.

The compositional dependence of the volume of hydrates is solely in the  $v_0$  term. The compositional dependence was assumed to be a Langmuir type expression that accounts for a guest molecules repulsive nature with each hydrate

---

**TABLE 5.4**  
**Regressed Volumetric Thermal Expansion**  
**Parameters for Hydrate Volume (Divide by 3**  
**to Get Linear Thermal Expansion Parameters)**

Hydrate	$\alpha_1$ (K <sup>-1</sup> )	$\alpha_2$ (K <sup>-2</sup> )	$\alpha_3$ (K <sup>-3</sup> )
sI	3.384960E-4	5.400990E-7	-4.769460E-11
sII	2.029776E-4	1.851168E-7	-1.879455E-10
sH	3.575490E-4	6.294390E-7	0

---

cage. The general form of the equation for  $v_0$  is

$$v_0(x) = \left( a_0^* + \sum_i N_i \sum_J f(\theta_{iJ}) \Delta r_{iJ} \right)^3 \quad (5.36)$$

where  $N_i$  is the number cages of type  $i$  in the hydrate,  $\Delta r_{iJ}$  is the repulsive constant for guest molecule  $J$  in hydrate cage  $i$ , and  $a_0^*$  is denoted as the standard lattice parameter at  $T_0$ ,  $P_0$ , and some  $x_0$ . The standard lattice parameters for sI, sII, and sH hydrates were arbitrarily chosen to be 11.99245, 17.10000, and 11.09826 Å, respectively, such that  $v_0(\vec{x})$  is that of the standard, empty hydrates (derived from data). The function,  $f(\theta_{iJ})$ , is defined to be

$$f(\theta_{iJ}) = \frac{(1 + \eta_i)\theta_{iJ}}{1 + \eta_i\theta_{iJ}} \exp[D_J - \bar{D}] \quad (5.37)$$

for the  $5^{12}$  hydrate cage and

$$f(\theta_{iJ}) = \frac{(1 + \eta_i)\theta_{iJ}}{1 + \eta_i\theta_{iJ}} \quad (5.38)$$

for all other sI and sII hydrate cages ( $5^{12}6^2$  and  $5^{12}6^4$ ), where in Equations 5.37 and 5.38  $\eta_i$  is the coordination number of cage  $i$  ( $z_i$ ) per water molecule in the hydrate ( $N_i$ ),  $\theta_{iJ}$  is the fractional occupancy of component  $J$  in cage  $i$ ,  $D_J$  is the molecular diameter of component  $J$ , and  $\bar{D}$  is the fractional occupancy average molecular diameter of the guest molecules in the hydrate,

$$\bar{D} = \sum_J D_J \theta_{iJ}$$

Guests larger than ethane cannot fit into the small cage of sII and therefore the repulsive constants are zero. Due to the lack of sI compositional data, the repulsive constant for only one of the hydrate cages could be regressed. Due to lack of sH compositional data, the volume of sH hydrates was assumed to be independent of composition (Table 5.5).

The compressibility of a mixed hydrate (i.e., more than one guest molecule) is assumed to be of the form

$$\kappa_H = \sum_{J=1}^C \kappa_{JH} \theta_{JL} \quad (5.39)$$

where  $\theta_{JL}$  is the fractional occupancy of hydrate guest  $J$  in the large cage. Note that for sH hydrates, no experimental compressibility data exists. Therefore, the linear compressibility of the sH hydrate,  $\kappa_{sH}$ , is assumed to be 1E-7 bar<sup>-1</sup>. Table 5.6 lists all compressibility parameters used in the hydrate volume model.

The standard hydrates of sI, sII, and sH were assumed to be the empty hydrates of methane, propane, and methane + neohexane, respectively. While the thermal expansion parameters are the same for the real and standard hydrates, the compressibility parameter and standard volume are not. The volumetric compressibility of the standard hydrates of sI, sII, and sH are 3E-5, 3E-6, and 3E-7,

**TABLE 5.5**  
**Regressed Repulsive Constants and Guest Diameters for Hydrate Volume**

Component	Diameter (Å)	sI small	sI large	sII small	sII large
Methane	4.247	1.7668E-2	1.0316E-2	2.0998E-3	1.1383E-2
Ethylene	4.816	0	1.5773E-2	2.3814E-3	1.3528E-2
Ethane	5.076	0	2.5154E-2	2.5097E-3	1.4973E-2
Propylene	5.522	0	2.9839E-2	0	2.1346E-2
Propane	5.745	0	0	0	2.5576E-2
n-Butane	6.336	0	0	0	3.6593E-2
i-Butane	6.306	0	0	0	3.6000E-2
i-Pentane	6.777	0	0	0	4.7632E-2
Benzene	6.272	0	0	0	3.5229E-2
Nitrogen	4.177	1.7377E-2	0	2.0652E-3	1.1295E-2
H <sub>2</sub> S	4.308	1.7921E-2	0	2.1299E-3	1.1350E-2
CO <sub>2</sub>	4.603	0	5.8282E-3	2.2758E-3	1.2242E-2
Xenon	4.404	1.8321E-2	0	2.1774E-3	1.1524E-2

**TABLE 5.6**  
**Regressed Linear Compressibility Parameters  
 for Hydrate Volume (Multiply by 3 to Get  
 Volumetric Compressibility Parameters)**

Component	sI (bar <sup>-1</sup> )	sII (bar <sup>-1</sup> )
Methane	1.0E-05	5.0E-05
Ethylene	2.2E-06	2.2E-05
Ethane	1.0E-08	1.0E-07
Propylene	1.0E-07	1.0E-06
Propane	1.0E-07	1.0E-06
n-Butane	NA	1.0E-08
i-Butane	NA	1.0E-08
i-Pentane	NA	1.0E-08
Benzene	NA	1.0E-08
Nitrogen	1.1E-05	1.1E-05
H <sub>2</sub> S	5.0E-06	1.0E-05
CO <sub>2</sub>	1.0E-06	1.0E-05
Xenon	9.0E-06	1.0E-05

respectively. The standard volumes for each are 22.7712, 22.9456, and 24.2126 cm<sup>3</sup>/mol, respectively. Note that the standard volumes were converted from the standard lattice parameters given earlier based on structure and corresponding number of water molecules in the hydrate lattice.

**TABLE 5.7**  
**Regressed Formation Properties of Standard Hydrates**

Property	sI	sII	sH
$g_{w_0}^\beta$ (J/mol)	-235537.85	-235627.53	-235491.02
$h_{w_0}^\beta$ (J/mol)	-291758.77	-292044.10	-291979.26
$A$ (J/cm <sup>3</sup> )	25.74	260.00	0
$B$ (J/cm <sup>3</sup> )	-481.32	-68.64	0

The other regressed properties for the method are found in Tables 5.7 and 5.8. The parameters listed in this monograph are a result of a multivariate Gauss–Newton optimization by Ballard (2002) to which the reader should refer if a more detailed explanation of the method and fitted parameters is required.

Because there are a number of equations above, an equation summary is given in Table 5.9 to calculate the fugacity of water in hydrates.

### 5.1.7 The Gibbs Free Energy Method

This section is based on Ballard's (2002) extension of the ground-breaking work in Bishnoi's group by Gupta (1990). To calculate thermodynamic equilibrium for a closed system, three fundamental conditions must be met:

1. Temperature equilibrium of all phases,
2. Pressure equilibrium of all phases, and
3. Equality of chemical potential of a component in each phase,

all resulting from the Gibbs energy being at a minimum (Gibbs, 1928). These conditions are commonly used in developing procedures for solving for thermodynamic equilibrium. For a system of known phases, meeting the first three conditions will ensure that the Gibbs energy is at a minimum. The most common implementation of these conditions is for the two-phase system, vapor and liquid hydrocarbon, known as the vapor liquid equilibrium (VLE) flash.

The requirement that the Gibbs energy of the system must be at a minimum, at a given temperature and pressure, is a statement of the second law of thermodynamics. Meeting conditions (1) to (3) is necessary for thermodynamic equilibrium but is not sufficient for the minimization of the Gibbs energy. Baker et al. (1982) discuss this further in their development of a solution procedure for multiphase equilibrium calculations. For simple systems in which the phases present at equilibrium are known (i.e., vapor and liquid hydrocarbon), however, conditions (1) through (3) are commonly used without difficulty. When solving for thermodynamic equilibrium in a more complex system in which several phases could form, a fourth criterion, the minimum of Gibbs energy, may be used.

**TABLE 5.8**  
**Regressed Kihara Potential Parameters (“*a*” as in Original Reference)**

Component	<i>a</i> (Å)	<i>σ</i> (Å)	<i>ε/k</i> (K)
Methane	0.3834	3.14393	155.593
Ethylene	0.4700	3.24461	180.664
Ethane	0.5651	3.24693	188.181
Propylene	0.6500	3.33039	186.082
Propane	0.6502	3.41670	192.855
n-Butane	0.9379	3.51726	197.254
i-Butane	0.8706	3.41691	198.333
i-Pentane	0.9868	3.54550	199.560
Benzene	1.2000	3.25176	223.802
2,3-Dimethyl-1-butene	1.0175	3.55376	211.924
3,3-Dimethyl-1-butene	0.7773	3.56184	253.681
Methylcyclopentane	1.0054	3.56878	229.928
Neohexane	1.0481	3.54932	229.832
2,3-Dimethylbutane	1.0790	3.57910	210.664
Cycloheptane	1.0576	3.59028	250.187
Ethylcyclopentane	1.1401	3.60425	219.083
Methylcyclohexane	1.0693	3.58776	237.989
2,2,3-Trimethylbutane	1.1288	3.59955	232.444
2,2-Dimethylpentane	1.2134	3.59989	224.609
3,3-Dimethylpentane	1.2219	3.59117	204.968
cis-1,2-Dimethylcyclohexane	1.1494	3.60555	233.510
1,1-Dimethylcyclohexane	1.1440	3.60212	246.996
Ethylcyclohexane	1.1606	3.60932	220.527
Nitrogen	0.3526	3.13512	127.426
Hydrogen sulfide	0.3600	3.10000	212.047
Carbon dioxide	0.6805	2.97638	175.405
Xenon	0.2357	3.32968	193.708

That is, if the amount of phases present at the solution is not known *a priori*, the Gibbs energy must be used to determine what phases are present.

Implementation of conditions (1) to (3) is done following a similar procedure as that of a two-phase system (Rachford and Rice, 1952). For a system with *C* components and  $\pi$  possible phases, satisfying a simple mass balance for each component in each phase results in the following objective function:

$$E_k = \sum_{i=1}^C \frac{z_i(x_{ik}/x_{ir} - 1)}{1 + \sum_{\substack{j=1 \\ j \neq r}}^{\pi} \alpha_j(x_{ij}/x_{ir} - 1)} = 0, \quad k = 1, \dots, \pi \quad (5.40)$$

where  $z_i$  is the mole fraction of component *i* in the feed,  $\alpha_j$  is the molar phase fraction of phase *j*, and  $x_{ik}$  is the mole fraction of component *i* in phase *k*.

**TABLE 5.9**  
**Equation Summary to Determine Fugacity of Water in Hydrate**

$$f_w^H = f_{w,0} \exp \left[ \frac{\mu_w^H - g_{w,0}}{RT} \right] \quad (5.32)$$

where  $f_{w,0}$  is 1 bar,  $g_{w,0}$  is the Gibbs energy of pure water in the ideal gas state at 1 bar

$$\mu_w^H = g_w^\beta + RT \sum_i v_i \ln \left( 1 - \sum_J \theta_{iJ} \right) + RT \ln \gamma_w^H \quad (5.28)$$

$$\theta_{iJ} = \frac{C_{iJ} f_J}{1 + C_{iJ} f_J} \quad (5.22c)$$

$$C_{J,i} = \frac{4\pi}{kT} \int_0^{R_1-a_J} \exp \left[ -\frac{\sum_n \omega_{J,n}(r)}{kT} \right] r^2 dr \quad (5.27b)$$

$$\varpi_{Jn}(r) = 2z_n \varepsilon_J \left[ \frac{\sigma_J^{12}}{R_n^{11} r} \left( \delta^{10} + \frac{a_J}{R_n} \delta^{11} \right) - \frac{\sigma_J^6}{R_n^5 r} \left( \delta^4 + \frac{a_J}{R_n} \delta^5 \right) \right] \quad (5.25a)$$

$$\text{where } \delta^N = \frac{1}{N} \left[ \left( 1 - \frac{r}{R_n} - \frac{a_J}{R_n} \right)^{-N} - \left( 1 + \frac{r}{R_n} - \frac{a_J}{R_n} \right)^{-N} \right] \quad (5.25b)$$

$$\frac{g_w^\beta}{RT} = \frac{g_{w,0}^\beta}{RT_0} - \int_{T_0}^T \frac{h_w^\beta}{RT^2} dT + \int_{P_0}^P \frac{v_w^\beta}{RT} dP \quad (5.33)$$

$$h_w^\beta = h_{w,0}^\beta + \int_{T_0}^T c_{P_w^\beta} dT \quad (5.34)$$

$$v_w^\beta = (a_0^*)^3 \exp[\alpha_1(T - T_0) + \alpha_2(T - T_0)^2 + \alpha_3(T - T_0)^3 - \kappa(P - P_0)]$$

$$\ln \gamma_w^H = \frac{\Delta g_{w,0}^\beta}{RT_0} + \frac{\Delta h_{w,0}^\beta}{R} \left( \frac{1}{T} - \frac{1}{T_0} \right) + \int_{P_0}^P \frac{\Delta v^H}{RT} dP \quad (5.31)$$

$$\Delta g_{w,0}^\beta = a \Delta v_0^H \quad \text{and} \quad \Delta h_{w,0}^\beta = b \Delta v_0^H$$

$$\Delta v^H = v^H - v^\beta$$

$$v^H = v_0 \exp[\alpha_1(T - T_0) + \alpha_2(T - T_0)^2 + \alpha_3(T - T_0)^3 - k(P - P_0)] \quad (5.35)$$

$$v_0(\vec{x}) = \left( a_0^* + \sum_i N_i \sum_J f(\theta_{iJ}) \Delta r_{iJ} \right)^3 \quad (5.36)$$

$$5^{12} \text{ cages: } f(\theta_{iJ}) = \frac{(1 + \eta_i)\theta_{iJ}}{1 + \eta_i\theta_{iJ}} \exp[D_J - \bar{D}] \quad (5.37)$$

$$5^{12}6^2 \text{ and } 5^{12}6^4 \text{ cages: } f(\theta_{iJ}) = \frac{(1 + \eta_i)\theta_{iJ}}{1 + \eta_i\theta_{iJ}} \quad (5.38)$$

$$\kappa_H = \sum_{J=1}^C \kappa_{JH} \theta_{JL} \quad (5.39)$$

The subscript  $r$  refers to a reference phase, which is present at thermodynamic equilibrium. Implementation of conditions (1) to (3) results in the following expression for the mole fraction ratio:

$$\frac{x_{ik}}{x_{ir}} = \frac{\phi_{ir}}{\phi_{ik}} = K_{ik} \quad i = 1, \dots, C \quad k = 1, \dots, \pi \quad (5.41)$$

where  $K_{ik}$  is the distribution coefficient, and  $\phi$  is the fugacity coefficient. Note that the definition of the distribution coefficient (Equation 5.41) is valid only for phases present at thermodynamic equilibrium. Therefore, this approach can only be used if all phases ( $k = 1, \dots, \pi$ ) are present. This is quite a drawback in that, for natural gases and water, the phases present at equilibrium are usually not known.

Gupta (1990) showed that, by defining the mole fraction ratio in terms of the distribution coefficient as

$$\frac{x_{ik}}{x_{ir}} = \frac{\phi_{ir}}{\phi_{ik}} e^{y_k} = K_{ik} e^{y_k} \quad i = 1, \dots, C \quad k = 1, \dots, \pi \quad (5.42)$$

where  $y_k$  is defined as

$$y_k = \ln \left( \frac{f_{ik}}{f_{ir}} \right) \quad k = 1, \dots, \pi \quad (5.43)$$

is equivalent to minimizing the Gibbs energy of the system conditional to

$$S_k = \frac{\alpha_k y_k}{\alpha_k + y_k} = 0 \quad k = 1, \dots, \pi \quad (5.44)$$

That is, if  $\alpha_k > 0$  then phase  $k$  is present and  $y_k = 0$  and likewise, if  $\alpha_k = 0$  then phase  $k$  is not present and  $y_k \neq 0$ . Note that Equation 5.44 is always satisfied for the reference phase by definition of  $y_k$ .

Replacing the mole fraction ratio in Equation 5.40 with Equation 5.42, we obtain

$$E_k = \sum_{i=1}^C \frac{z_i (K_{ik} e^{y_k} - 1)}{1 + \sum_{\substack{j=1 \\ j \neq r}}^{\pi} \alpha_j (K_{ij} e^{y_j} - 1)} = 0 \quad k = 1, \dots, \pi \quad (5.45)$$

which is valid for all phases (present or not) at a solution. Equation 5.45 is used to determine the set of phase amounts,  $\alpha_k$ , and stability variables,  $y_k$ , that satisfy thermodynamic equilibrium.

The solution procedure is split into two parts: (1) minimizing Gibbs energy by updating phase amounts and stability variables at a given set of  $K$ -values and (2) updating  $K$ -values at a given set of phase amounts and stability variables. This approach is typical in phase equilibrium problems. The Newton procedure is

used to minimize the Gibbs energy of the system at a given set of  $K$ -values (via Equation 5.45). This approach is convergent as long as the fugacity coefficients are not strong functions of composition. This is certainly the case for the fluid phases such as vapor and liquid hydrocarbon but is not necessarily true for the aqueous and hydrate phases. With proper care this approach is convergent for all systems.

The Newton method gives a correction to the phase amounts and stability variables based on the gradient of the Gibbs energy at the given set of  $K$ -values. Due to the highly nonideal behavior of the hydrate phases, all corrections are scaled such that no phase amount or stability variable is changed more than 25% of its original value. That is, the entire correction vector is scaled so as to keep the proper direction of convergence.

In the development of Equation 5.45, the composition of each phase is given as

$$x_{ik} = \frac{z_i K_{ik} e^{y_k}}{1 + \sum_{\substack{j=1 \\ j \neq r}}^{\pi} \alpha_j (K_{ij} e^{y_j} - 1)} \quad i = 1, \dots, C \quad k = 1, \dots, \pi \quad (5.46)$$

Equation 5.46 is used to update the composition of each phase. With the new composition, the fugacity coefficients are calculated to get the new set of  $K$ -values. As is the case for minimizing the Gibbs energy, this approach is convergent as long as the fugacity coefficients are not strong functions of composition. Successive substitution of the composition gives linear convergence whereas Newton's method gives quadratic convergence.

Due to the highly nonideal behavior of the hydrate phases, Equation 5.46 is not used to update the hydrate composition. However, the compositions of all nonhydrate phases are determined via Equation 5.46. All composition corrections of a given phase are scaled such that no composition in that phase is changed by more than 50% of its original value. The expression for the composition of species in the hydrate follows from a simple mass balance:

$$x_{iH} = \frac{\sum_m v_m \theta_{im}}{1 + \sum_m \sum_j v_m \theta_{jm}} \quad (5.47)$$

where  $v_m$  is the number of hydrate cages of type  $m$  per water molecule in the hydrate. This equation is used in place of Equation 5.46 to update the hydrate phase composition.

The solution procedures discussed above are implemented into the algorithm shown in [Figure 5.6](#).

As can be seen in Figure 5.6, thermodynamic equilibrium is achieved when the Gibbs energy is at a minimum ( $E_k = 0$ ) and the difference in the updated mole fractions and previous mole fractions ( $\Delta x_{ik}$ ) for each phase is less than 1E-6. One of the crucial steps in obtaining a solution is creating a “good” initial estimate for the unknown variables.

Several authors have determined ideal  $K$ -values for component distribution between V-L<sub>hc</sub> (DePriester, 1953; Hadden and Grayson, 1961) and V-Hydrate

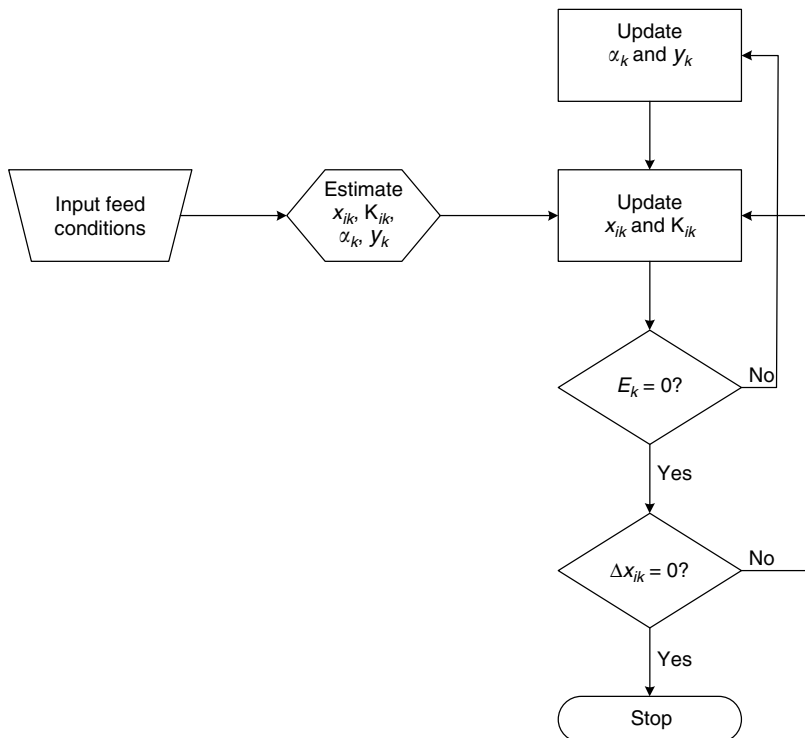


**FIGURE 5.6** Algorithm to solve for thermodynamic equilibrium.

(Wilcox et al., 1941) phases. However, Ballard (2002) developed composition-independent sets of  $K$ -values to provide the initial estimate for the component distribution between all possible phases: vapor, liquid hydrocarbon, aqueous, sI hydrate, sII hydrate, sH hydrate, ice, solid NaCl, solid KCl, and solid CaCl<sub>2</sub>.

The thesis of Ballard (2002) details this calculation method, which includes multiphase systems, solid phases including ice and salts, and thermodynamic inhibition. The CSMGem (the last three initials are the first letters of “Gibbs energy minimization”) User’s Manual, included in the CD in the endpapers, and the examples of hydrate calculation shown in the [Appendix A](#), enable the reader to use the CD programs.

The Gibbs energy minimization method allows for calculations of the formation conditions for any phase (including the hydrate). It also allows for the calculation of phases present at any  $T$  and  $P$  (whether hydrates are present or not). Therefore, included are the options to perform all thermodynamic calculations with every phase and not just the hydrate. The types of calculations, combined with plotting capability, included in CSMGem are

1. Hydrate formation temperature and pressure (with and without inhibition)

2. Formation temperature and pressure of phases other than hydrates
3. Flashes (phase compositions/amounts) at a temperature and pressure
4. Multiphase calculations (from two to eight phases)
5. Expansion through a valve or turboexpander.

### 5.1.8 Accuracy of CSMGem Compared to Commercial Hydrate Programs

A comparison of predictions from CSMGem, the program included in the CD of this work, with the second edition's version (CSMHYD) and three commercial hydrate prediction programs, is given here for all recent hydrate data reported in literature. The five programs (with the last three commercial) compared in this work are

CSMGem—Colorado School of Mines (2007 edition)

CSMHYD—Colorado School of Mines (1998 edition)

DBRHhydrate—DBRobinson Software Inc. (version 5.0)

Multiflash—Infochem Computer Services Ltd. (version 3.0)

PVTsim—Calsep A/S (version 11)

The comparisons are broken into two categories for hydrate formation temperatures and pressures (1) uninhibited systems, and (2) thermodynamically inhibited systems. These comparisons show the accuracy that may be expected from readily available hydrate prediction programs. A detailed comparison of the accuracy of these programs is given by Ballard and Sloan (2004b).

A series of figures follows, giving the average errors in temperature and pressure for several types of hydrates based on the following categories: (1) single guest or simple hydrates, (2) binary guest hydrates, (3) ternary guest hydrates, (4) multicomponent hydrates (natural gas hydrates), (5) hydrates in black oils (BO) and gas condensates (GC), and (6) sH hydrates. The results are given as the average error either in temperature or pressure. The average absolute error in temperature and pressure are calculated as:

$$T_{\text{Error}} = \frac{\sum_{\# \text{ data points}} |T_{\text{predicted}} - T_{\text{experimental}}|}{\# \text{ data points}} \quad (5.48)$$

$$P_{\text{Error}} = \frac{\sum_{\# \text{ data points}} |P_{\text{predicted}} - P_{\text{experimental}}| / P_{\text{experimental}}}{\# \text{ data points}} \cdot 100\% \quad (5.49)$$

and are given in Kelvin and any pressure units, respectively.

[Figures 5.7](#) and [5.8](#) give the values for all available uninhibited hydrate data (listed in [Chapter 6](#)), comparing the accuracies of the five programs.

From Figures 5.7 and 5.8, it is apparent that more reliable thermodynamic data are needed, particularly for the (1) BO and GC, and (2) Natural gas systems.

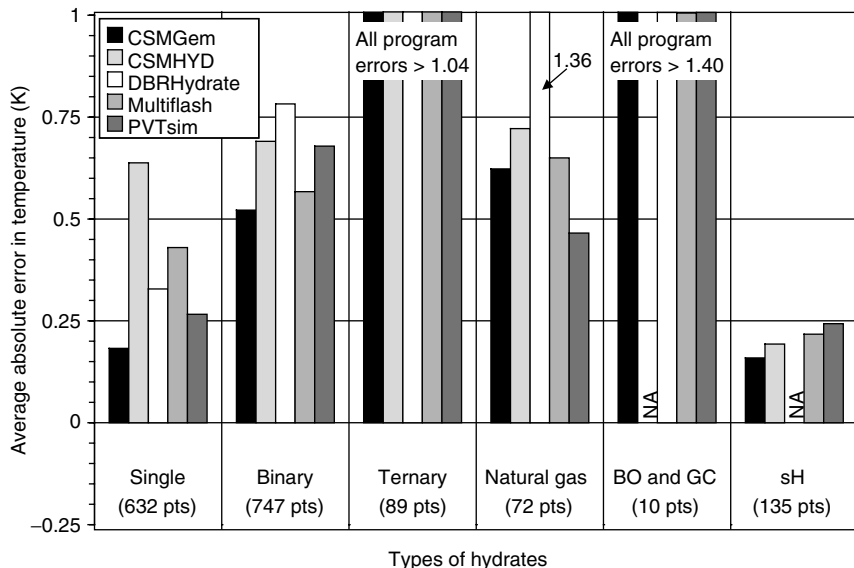


**FIGURE 5.7** Incipient temperature accuracy (absolute) for uninhibited hydrate data for five programs.

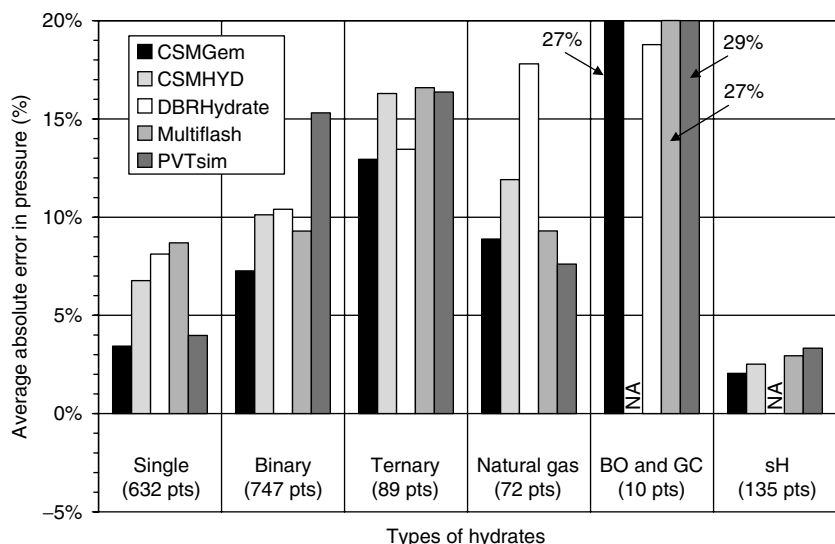


**FIGURE 5.8** Incipient pressure accuracy (absolute) for uninhibited hydrate data for five programs.

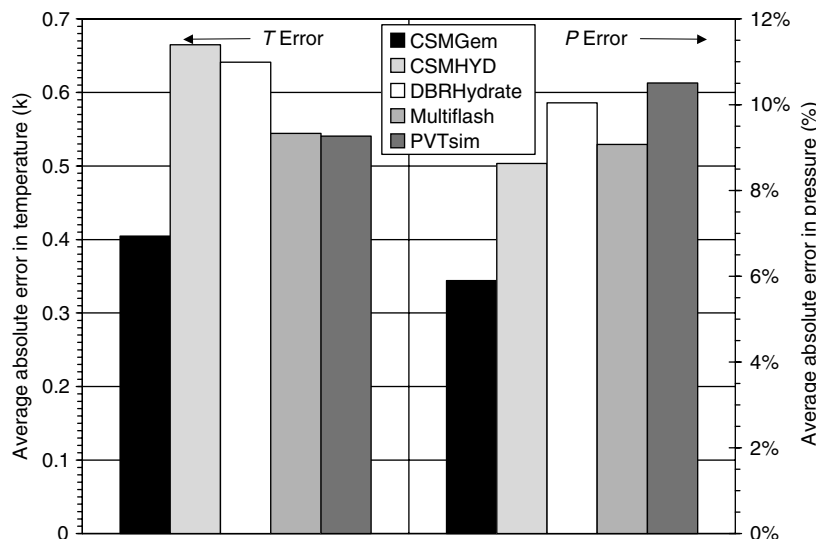


**FIGURE 5.9** Uninhibited incipient hydrate  $T$  and  $P$  errors (absolute) for all hydrates (1685 pts).

Figure 5.9 suggests the rule-of-thumb that one can expect the incipient hydrate temperature and pressure to be predicted to within 0.65 K and 10% of overall pressure, respectively. These values approximate the experimental accuracy of the measurements, and suggest that it may not be practical to increase the prediction accuracy until further progress is required for measurement accuracy. Such comparisons with data suggest that hydrate phase equilibria predictions are sufficiently established to permit the state-of-the-art to turn to time dependent phenomena (Sloan, 2005).

For the second category, consider a comparison of available programs to thermodynamically inhibited incipient hydrate data, in Figures 5.10 and 5.11.

Figures 5.10 and 5.11 show that one may expect modern programs to predict the methanol- and NaCl-inhibited incipient temperature and pressure to within about 2 K and 20% in pressure, respectively. While comparisons for monoethylene glycol are not given, they might be comparable for low concentrations, such as below 30 wt% in free water. Second, the two figures show that the inaccuracies of mixtures of the two inhibitors (methanol and NaCl) are similar to that of the pure inhibitors.

### 5.1.9 *Ab Initio* Methods and the van der Waals and Platteeuw Method

Recently there has been a concerted effort to calculate potentials between the atoms and molecules in hydrates, using *ab initio* methods or quantum mechanics, initiated

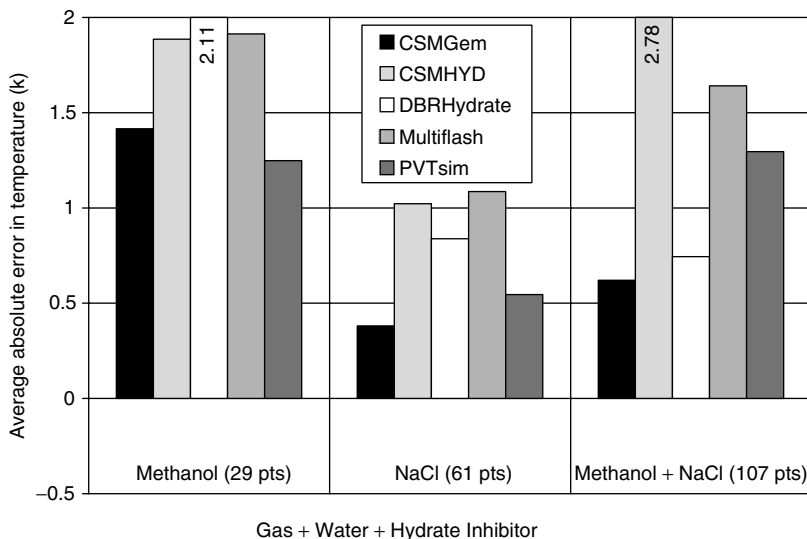


**FIGURE 5.10** Hydrate formation  $T$  error (absolute) for all inhibited hydrates.

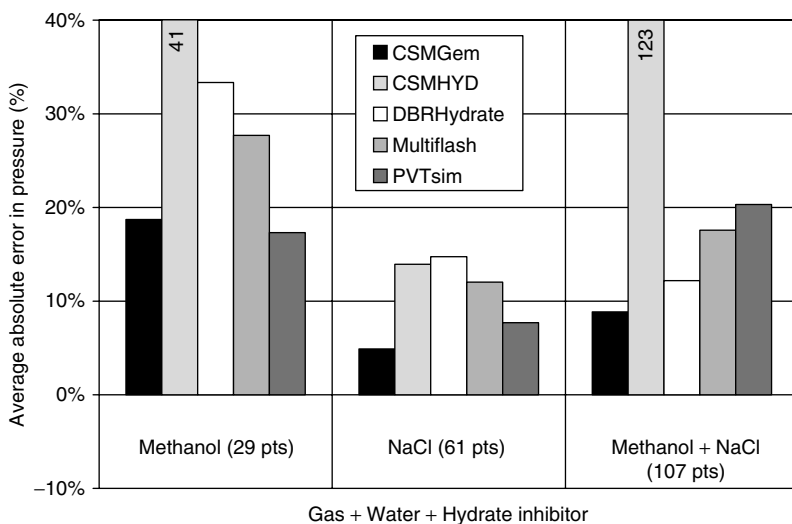


**FIGURE 5.11** Hydrate formation  $P$  error (absolute) for all inhibited hydrates.

with the Schrödinger equation. These methods are enabled by greatly enhanced computing capability over the last decade. Three doctoral theses are notable in this regard (1) Cao (2002), (2) Klauda (2003), and (3) Anderson (2005); the second thesis is from the group of Sandler at the University of Delaware, and the first and last theses were developed via collaborations of Tester with the group of Trout at

the Massachusetts Institute of Technology. The thesis of Cao is considered as the fundamental *ab initio* groundwork, so only the advances of Klauda and Anderson are discussed here.

Some advantages of the *ab initio* methods are

1. Potential parameters (such as the Kihara core or Lennard-Jones potentials of the previous sections) can be calculated from a small set of fundamental, *ab initio* intermolecular energies, rather than fits of the potentials to phase equilibria and spectroscopic data.
2. Potential parameters are well-defined and do not extend over a wide range of values.
3. Nonspherical shells are readily included in generating the Langmuir constants.
4. Water molecules beyond the first shell are readily included in Langmuir constants.
5. Guest–guest interactions between cages can be easily included.
6. Critical hydrate parameters, such as cage occupancies and structural transitions can be predicted *a priori*, without fitting the model to spectroscopic measurements.

The above advantages remove three of the major assumptions in the van der Waals and Platteeuw model—namely Assumptions 3 and 4 in Section 5.1.1, as well as Assumption 6 in Section 5.1.4. The three theses show that, in principle, the *ab initio* methods have the potential to compose the largest improvements to the van der Waals and Platteeuw theory in the last half-century. For cases with a few components, it can be shown that *ab initio* methods represent an improvement over common methods (Anderson et al., 2005), such as the program CSMHYD, which accompanied the second, 1998 edition of this book.

However, there are several pragmatic restrictions of the *ab initio* methods for natural gas mixtures which cause them to be currently less applicable than the programs composed in Section 5.1.8, and included in the endpapers CD . Most concerns originate in the fact that computer capacity, time, and effort limit the exact application of the Schrödinger equation between all of the atoms present in the system:

1. It is only practical to calculate the interaction between the guest atoms and a partial cage, typically five or ten water molecules, and then apply some configurational procedure to account for the remainder,
2. The principle of the calculation is shown to be more accurate than previously available programs such as CSMHYD (included with the second edition of this book) using a subset of natural gas hydrate guest formers. For example Klauda (2003) calculated values for CH<sub>4</sub>, C<sub>2</sub>H<sub>6</sub>, C<sub>3</sub>H<sub>8</sub>, N<sub>2</sub>, and CO<sub>2</sub> their mixtures, but omitted n-C<sub>4</sub>H<sub>10</sub>, i-C<sub>4</sub>H<sub>10</sub>, H<sub>2</sub>S, and all structure H formers. For hydrocarbon guests, Anderson (2005) considered only CH<sub>4</sub>, C<sub>2</sub>H<sub>6</sub>, C<sub>3</sub>H<sub>8</sub>, and i-C<sub>4</sub>H<sub>10</sub>, without including noncombustibles, n-C<sub>4</sub>H<sub>10</sub>, or structure H formers.

3. Frequently, simple potentials such as Lennard-Jones potentials must be complicated by the inclusion of coulombic contribution parameters, as used for CO<sub>2</sub> and C<sub>3</sub>H<sub>8</sub> by Klauda, requiring other fitting parameters.
4. The methods have yet to be extended to common thermodynamic inhibitors such as methanol or monoethylene glycol. In principle the extension is not a function of the *ab initio* methods since the thermodynamic inhibitors affect the water activity; yet this extension has not been quantified.

In sum, *ab initio* methods are beginning to fulfill their substantial promise for hydrates. For many hydrate guest components, *ab initio* methods have been shown to extend some of the most fundamental calculations from quantum mechanics to macroscopic properties, and to predict spectroscopic hydrate properties acceptably.

Yet until these methods can be extended to all common natural gas guest components and their thermodynamic inhibitors, it will be difficult to use the programs pragmatically. To date the programs have proved the *ab initio* concept from an academic perspective. While extension of *ab initio* methods to all natural gas hydrate components can be done in principle, that task awaits the generation and maintenance of a complete program.

Until more complete *ab initio* hydrate programs are available for comparison with commonly used commercial hydrate programs, such as PVTSim, Multiflash, and DBRHhydrate, the use of the latter programs are likely to predominate.

## 5.2 APPLICATION OF THE METHOD TO ANALYZE SYSTEMS OF METHANE + ETHANE + PROPANE

Since mixtures of methane, ethane, and propane make up nearly 97 mol% of a typical natural gas mixture, the hydrate phase behavior of a natural gas mixture in contact with water will likely be approximated by that of a simple mixture of these three components in contact with water.

This chapter's statistical mechanics method was used to generate phase diagrams as illustrations of multicomponent hydrate equilibria concepts at one isotherm, 277.6 K, the most common temperature in a pipeline on the ocean floor at water depths beyond 600 m. Section 5.2.1 shows the fit if the method to single (simple) hydrates, before the extension to binary hydrate guests in Section 5.2.2. Section 5.2.3 shows the final extension to ternary mixtures of CH<sub>4</sub> + C<sub>2</sub>H<sub>6</sub> + C<sub>3</sub>H<sub>8</sub> and indicates an industrial application. Most of the discussion in this section was extracted from the thesis of Ballard (2002) and the paper by Ballard and Sloan (2001).

### 5.2.1 Pure Hydrate Phase Equilibria

Experimental data for hydrates of pure gases in contact with water are the most abundant, comprising of nearly 50% of all equilibrium hydrate-related data.

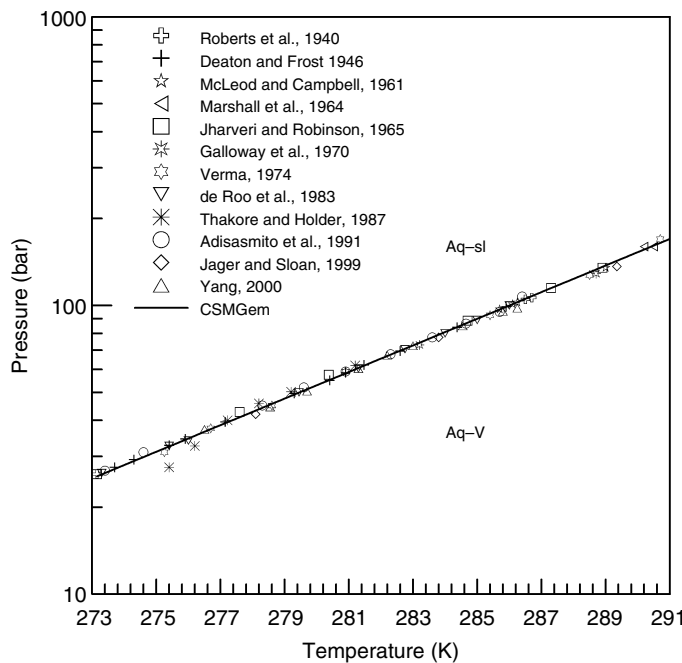


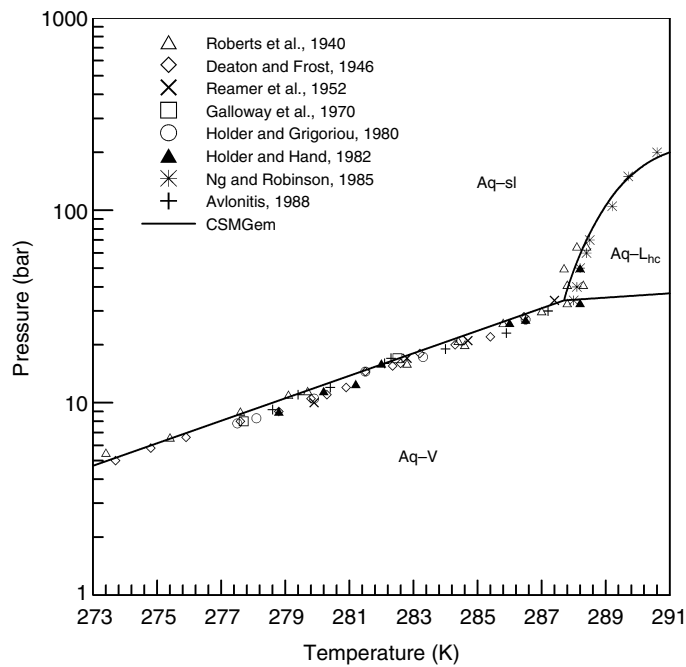
**FIGURE 5.12** Pressure vs. temperature diagram for methane + water system.

Although a typical natural gas is mainly comprised of the first three normal paraffins, the phase equilibria of each component with water will differ from that of a natural gas with water. However, a comparison of predictions with data for methane, ethane, and propane simple gas hydrates is given as a basis for understanding the phase equilibria of water with binary and ternary mixtures of those gases.

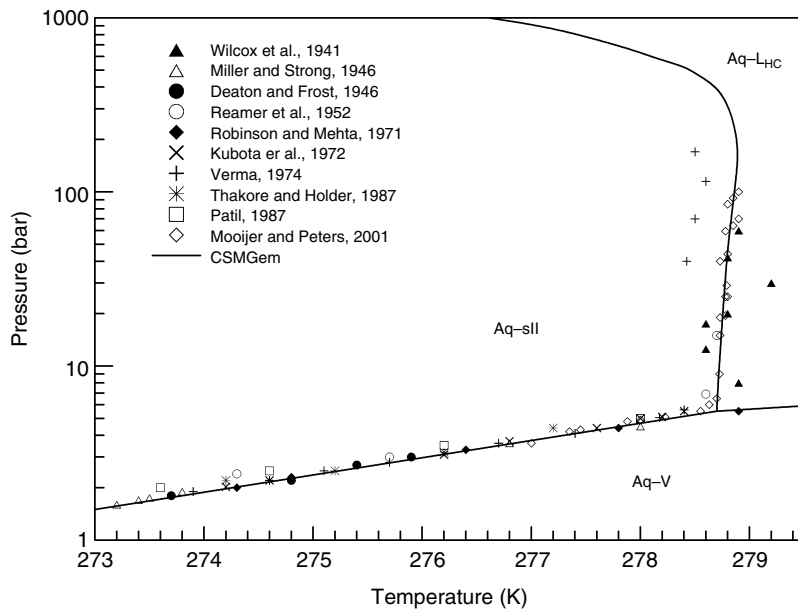
Figure 5.12 is the pressure versus temperature phase diagram for the methane + water system. Note that excess water is present so that, as hydrates form, all gas is incorporated into the hydrate phase. The phase equilibria of methane hydrates is well predicted as can be seen by a comparison of the prediction and data in Figure 5.12; note that the predicted hydrate formation pressure for methane hydrates at 277.6 K is 40.6 bar.

Figure 5.13 is the equivalent ethane + water pressure versus temperature phase diagram. Note that the Aq-sl-V line intersects the Aq-V-L<sub>hc</sub> line at 287.8 K and 35 bar. Due to differences in the volume and enthalpy of the vapor and liquid hydrocarbon, the three-phase hydrate formation line changes slope at high temperature and pressure from Aq-sl-V to Aq-sl-L<sub>hc</sub>, due to the intersection of Aq-sl-V line with the Aq-V-L<sub>hc</sub> line (slightly higher than the ethane vapor pressure). Note that the hydrate formation pressure for ethane hydrates at 277.6 K is predicted to be 8.2 bar.

Figure 5.14 is the propane + water pressure versus temperature phase diagram. Note that the data are scattered along the Aq-sII-L<sub>hc</sub> line due to difficulty



**FIGURE 5.13** Pressure vs. temperature diagram for ethane + water system.



**FIGURE 5.14** Pressure vs. temperature diagram for propane + water system.

measuring hydrate equilibria with three relatively incompressible phases. As with the ethane + water system in [Figure 5.13](#), the slope of the three-phase hydrate formation line changes drastically when the Aq-sII-V line intersects the Aq-V-L<sub>hc</sub> line. In fact, the Aq-sII-L<sub>hc</sub> line is nearly vertical but decreases to lower temperature at high pressure. The predictions suggest “pseudo-retrograde” phenomena for the propane hydrates in which the sII hydrate is predicted to dissociate by pressurization at a constant temperature.

For example, at 278.2 K, hydrates form at a pressure of approximately 5 bar and dissociate upon pressurization at approximately 600 bar. A more detailed explanation of the pseudo-retrograde hydrate phenomena can be found in the binary hydrates section which follows. Note that the hydrate formation pressure of propane hydrates along the Aq-sII-V line at 277.6 K is predicted to be 4.3 bar.

## 5.2.2 Binary Hydrate Phase Equilibria

To evaluate the phase equilibria of binary gas mixtures in contact with water, consider phase diagrams showing pressure versus pseudo-binary hydrocarbon composition. Water is present in excess throughout the phase diagrams and so the compositions of each phase is relative only to the hydrocarbon content. This type of analysis is particularly useful for hydrate phase equilibria since the distribution of the guests is of most importance. This section will discuss one diagram of each binary hydrate mixture of methane, ethane, and propane at a temperature of 277.6 K.

### 5.2.2.1 Methane + propane hydrates

[Figure 5.15](#) is the pseudo-binary pressure versus excess water composition diagram for the methane + propane + water system at a temperature of 277.6 K. At 277.6 K the hydrate formation pressures are 4.3 and 40.6 bar for pure propane (sII) and pure methane (sI) hydrates, respectively, as shown at the excess water composition extremes in Figure 5.15. As methane is added to pure propane, there will be a composition at which the incipient hydrate structure changes from sII to sI; as seen in the inset of Figure 5.15, this composition is predicted to be 0.9995 mole fraction methane in the vapor—a very small amount of propane added to a methane + water mixture will form sII hydrates.

As indicated in Example 4.1, note the dramatic decrease in hydrate pressure caused by a small amount of propane added to methane, due to the structure change (sI to sII). At pressures above incipient hydrate formation conditions, sII hydrates are predicted to be present throughout the entire composition range.

Of the possible binary combinations of methane, ethane, and propane, the methane + propane + water system ([Figure 5.15](#)) is the simplest.

### 5.2.2.2 Methane + ethane hydrates

Structural transitions (sI and sII) have been experimentally determined in the methane + ethane + water system via Raman, NMR, and diffraction between

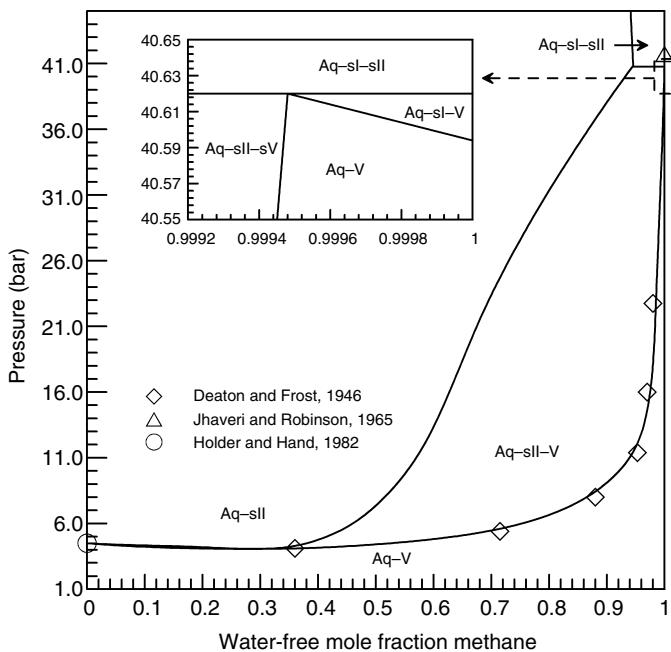


**FIGURE 5.15** Pseudo-*P*-*x* diagram for methane + propane + water system at 277.6 K.

0.736 and 0.994 mole fraction methane in the vapor at a temperature of 274.2 K (Subramanian et al., 2000a,b).

Figure 5.16 is the pseudo-binary pressure versus excess water composition diagram for the methane + ethane + water system at a temperature of 277.6 K. In the diagram, pure ethane and pure methane both form sI hydrates in the presence of water at pressures of 8.2 and 40.6 bar, respectively. Note that between the compositions of 0.74 and 0.994 mole fraction methane, sII hydrates form at the incipient formation pressure. Similar to the methane + propane + water system, only a small amount of ethane added to pure methane will form sII hydrates.

At pressures well above the incipient formation pressure, sII hydrates are predicted to be present in the composition range of 0.39–0.96 mole fraction methane. Regions in which sI and sII hydrates coexist in equilibrium are predicted in Figure 5.16. A physical explanation of why this occurs is that, as hydrates form, the vapor phase composition changes. If, for example, an excess water composition of 50 mol% methane and 50 mol% ethane is fed to a fixed volume at 277.6 K, sI hydrates will initially form at approximately 11 bar. Ethane, being the larger guest, will preferentially stabilize the large cages in the sI hydrate lattice so that the excess water composition of the hydrate will contain about 24 mol% methane and 76 mol% ethane (Figure 5.16).

As pressure is increased, the amount of sI hydrate in the system relative to vapor becomes larger, enriching the vapor with methane. This can be seen by applying

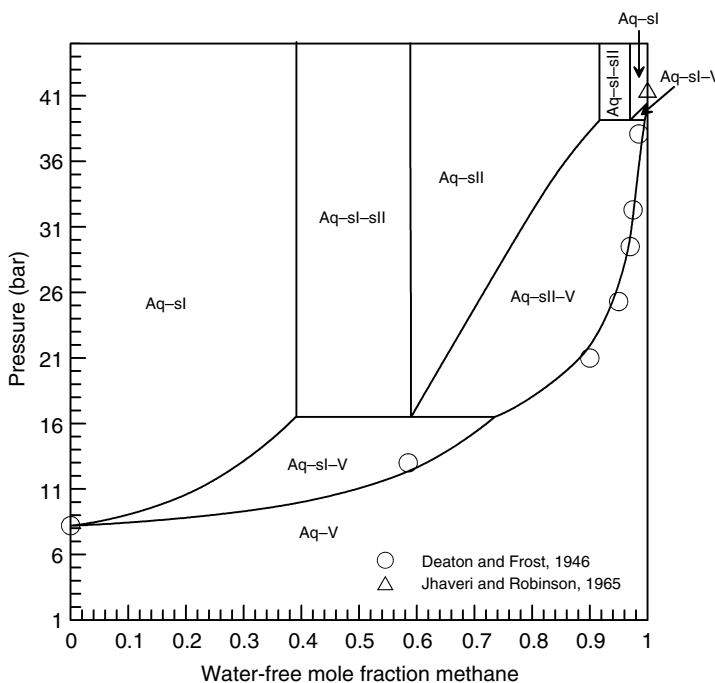


**FIGURE 5.16** Pseudo- $P$ - $x$  diagram for methane + ethane + water system at 277.6 K.

the inverse lever rule. At 16.5 bar, the vapor composition will be approximately 74 mol% methane, which is the vapor composition at which sII hydrates will form. It is at this condition (the horizontal line) where there are four phases (Aq-sI-sII-V) in the system; by Gibbs phase rule there is one degree of freedom, which is set by the temperature of the diagram (277.6 K). Therefore, as pressure is increased for a 50/50 mixture, the remaining vapor forms sII hydrates, leaving an aqueous phase, sI, and sII hydrates in the system. A similar sI + sII region is predicted at higher concentrations of methane (91.5–96.5 mol%) in which the initial hydrate structure is sII.

Figure 5.16 clearly shows the pressure and composition dependence of hydrate structure at a constant temperature. It can be seen that the hydrate can be sI, sII, or both depending on the composition and pressure. Predictions also show that there is temperature dependence as well.

While the effect is not shown in the Figure 5.16 isotherm, Table 5.10 shows the predicted effect of temperature on incipient hydrate structure for a excess water gas mixture of 73 mol% methane and 27 mol% ethane. As temperature increases, the incipient hydrate structure changes from sII to sI to sII and back to sI.

By Gibbs' Phase Rule, if pressure and composition of one phase are specified, the temperature must also be specified to determine which hydrate structure is present for three phases. As seen from Figure 5.16, there are many regions in which sI, sII, or both are present. Without the aid of program or a hydrate phase

**TABLE 5.10**  
**Effect of Temperature on Hydrate Structure  
 in the Methane (0.73) + Ethane (0.27) +  
 Water (Excess) System**

Temperature (K)	Incipient hydrate structure
273–275	sII
275–292	sI
292–301	sII
>301	sI

diagram, such as [Figure 5.16](#), generated by the Gibbs energy minimization flash program, it would be difficult to determine which phases are present. Assuming that the hydrate formed at the incipient conditions prevails at higher pressures and temperatures could be a costly mistake. In many practical situations such as flow assurance in natural gas pipelines and hydrates in oceanic and permafrost regions it is essential to know what phases are present. Subramanian et al. (2000a,b) discuss the practical applications of these predictions.

### 5.2.2.3 Ethane + propane hydrates

[Figure 5.17](#) shows a predicted pressure versus excess water composition plot for the ethane+propane+water system at 274 K. At 0.0 mol fraction ethane (propane+water) sII form at approximately 2 bar, and at 1.0 mol fraction ethane (ethane+water) sI form at approximately 5 bar. At the intermediate composition of 0.78 mole fraction ethane, a quadruple point (Aq–sI–sII–V) exists in which both incipient hydrate structures are in equilibrium with vapor and aqueous phase. This point will be referred to as the *structural transition composition*: the composition at which the incipient hydrate formation structure changes from sII to sI at a given temperature.

By the Gibbs phase rule, there is only one pressure at which Aq–sI–sII–V can coexist at a given temperature. Therefore, with an increase in pressure, the free vapor phase is completely converted into either sI or sII, depending on the feed composition of ethane and propane and which hydrate structure is present as illustrated in [Figure 5.17](#) pressures above incipient hydrate formation, phase regions are predicted to exist where both sI and sII hydrates are present.

[Figure 5.17](#) illustrates the effect on hydrate formation when ethane and propane are combined at constant temperature. Ethane acts as an inhibitor to sII formation due to competition of ethane with propane to occupy the large cages of sII. Propane also acts as an inhibitor to sI formation when added to ethane + water. In this case, however, since propane cannot enter the sI cavities, the fugacity of ethane is lowered as propane is added, destabilizing the sI hydrate. Holder (1976) refers to this inhibiting capacity as the “antifreeze” effect.

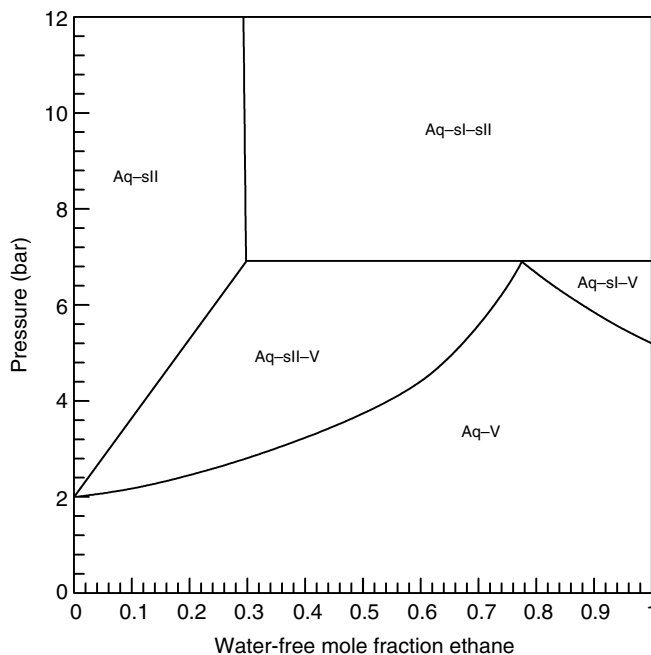


**FIGURE 5.17** Pseudo- $P$ - $x$  diagram for ethane + propane + water system at 274 K.

As the temperature is increased to 277.6 K the pressure versus composition diagram for the ethane + propane + water system changes drastically as shown in Figure 5.18. Between 0.0 and 0.6 mole fraction of ethane, the incipient hydrate structure is sII hydrate. However, if the pressure is increased to approximately 11.45 bar, between 0.3 and 0.6 mol fraction ethane, sII is predicted to dissociate to form an Aq-V-L<sub>hc</sub> region.

The pressure at which this dissociation is predicted to occur is called the *hydrate pseudo-retrograde pressure* at  $T$ . Pseudo-retrograde behavior is defined as the disappearance of a dense phase upon pressurization, which is counter-intuitive. This behavior resembles, but is not strictly the same as, vapor–liquid retrograde phenomena (de Loos, 1994).

The pseudo-retrograde pressure can be explained via evaluation of the vapor–liquid equilibria of ethane, propane, and water. The dashed line in Figure 5.18 is Aq-V-L<sub>hc</sub> envelope that would form if hydrates were not present. The Aq-sII-V phase region intersects the Aq-V-L<sub>hc</sub> region at the quadruple point (11.45 bar). According to Gibbs' Phase Rule there is one degree of freedom (three components, four phases), namely temperature which is set at 277.6 K. This point of intersection creates a four-phase line, Aq-sII-V-L<sub>hc</sub>, in the pseudo- $P$ - $x$  diagram. Therefore, the pressure at which the quadruple line occurs in Figure 5.18 is unique. That is, if pressure is increased, one of the phases must disappear. In this case, the sII phase dissociates and an Aq-V-L<sub>hc</sub> region remains.

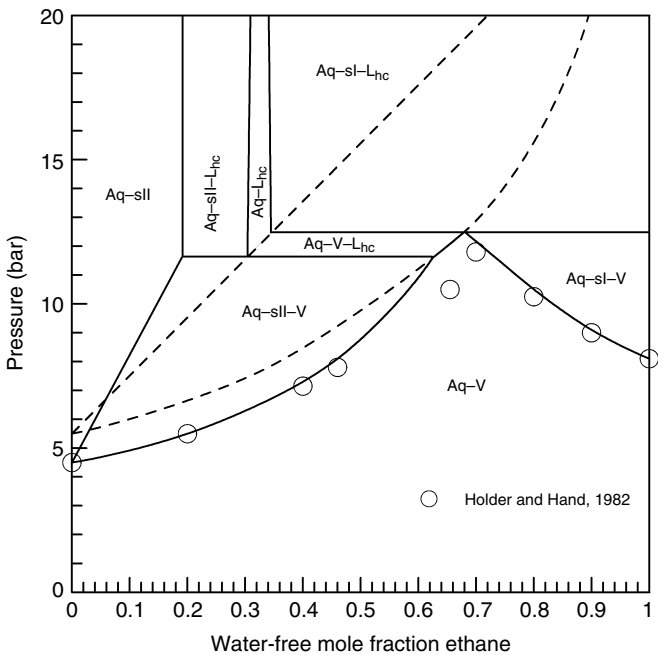
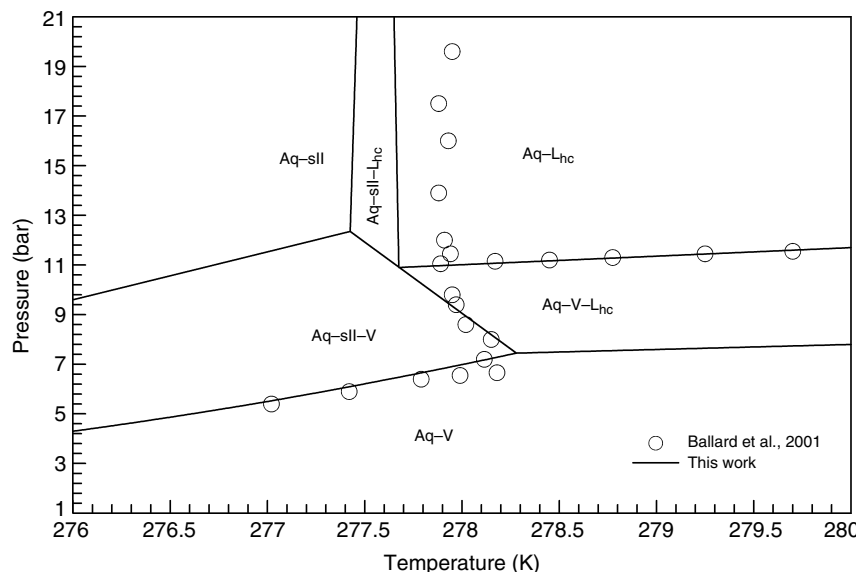


FIGURE 5.18 Pseudo- $P$ - $x$  diagram for ethane + propane + water system at 277.6 K.

The validity of the predictions in Figure 5.18 can be shown with a comparison of the data taken by Holder and Hand (1982) for this system. The sI and sII hydrate formation data points all compare quite well with the predictions with the exception of the point at 0.66 mole fraction ethane. Holder and Hand state that the data point at 0.66 mole fraction is sII but note that it could be at Aq-sII-V-L<sub>hc</sub> conditions. The predictions in Figure 5.18 support their observation of possible four-phase conditions but suggest that the data point may be at metastable Aq-sII-V-L<sub>hc</sub> conditions.

To test the predictions, experiments were carried out at the Delft University of Technology (TUD) (Ballard et al., 2001). In CSMGem, the pressure versus temperature phase diagram was generated using the model and then confirmed by experimental data. Figure 5.19 is the pressure versus temperature diagram for a 30/70 mixture of ethane and propane in contact with excess water.

Pseudo-retrograde phenomena are predicted to occur between the temperatures of 277.6 and 278.3 K. With a pressure increase of up to 5 bar, sII hydrates will dissociate at any temperature in this range. The lines are model predictions and the circles are experimental observations of hydrate dissociation obtained in the TUD laboratory. As can be seen in Figure 5.19, the TUD hydrate dissociation data do confirm the pseudo-retrograde melting. However, note that the Aq-sII-L<sub>hc</sub> predictions deviate 0.2 K from the data. It is usually assumed that hydrates never dissociate with an increase in pressure. However, both measurements and



**FIGURE 5.19**  $P$  versus  $T$  phase diagram for ethane (0.3) + propane (0.7) + water (excess) system with pseudo-retrograde phenomena.

predictions show, however, that for a wide excess water composition range, slight increases in pressure will result in the dissociation of sII hydrates (pseudo-retrograde dissociation) at low pressures ( $\sim 7$ –11 bar) near a temperature of 278 K. Pseudo-retrograde hydrate behavior was also predicted in the ethane + i-butane + water and ethane + propane + decane + water systems as well (Ballard et al., 2001), but are not shown here due to space constraints.

#### 5.2.2.4 Ternary hydrate phase equilibria and industrial application

With the phase equilibria of pure and binary hydrates discussed, the next step is to consider phase equilibria of the ternary gas mixture with water. For illustrative purposes only one pseudo-ternary phase diagram is presented at a temperature of 277.6 K and a pressure of 10.13 bar. The pseudo-ternary phase diagram is similar to true ternary phase diagrams except that water is in excess and therefore all compositions are given on a excess water basis. The pseudo-ternary phase diagrams is a composite of the phase diagrams discussed earlier:  $P$ - $T$  diagrams for the pure hydrates and pseudo- $P$ - $x$  diagrams for the binary hydrates. That is, the corners represent the intersection of an isotherm and isobar in the pure hydrate  $P$ - $T$  diagrams while the edges represent an isobar in the pseudo- $P$ - $x$  phase diagrams at 277.6 K.

Figure 5.20 is a pseudo-ternary phase diagram for the methane + ethane + propane + water system at a temperature and pressure of 277.6 K and 10.13 bar,

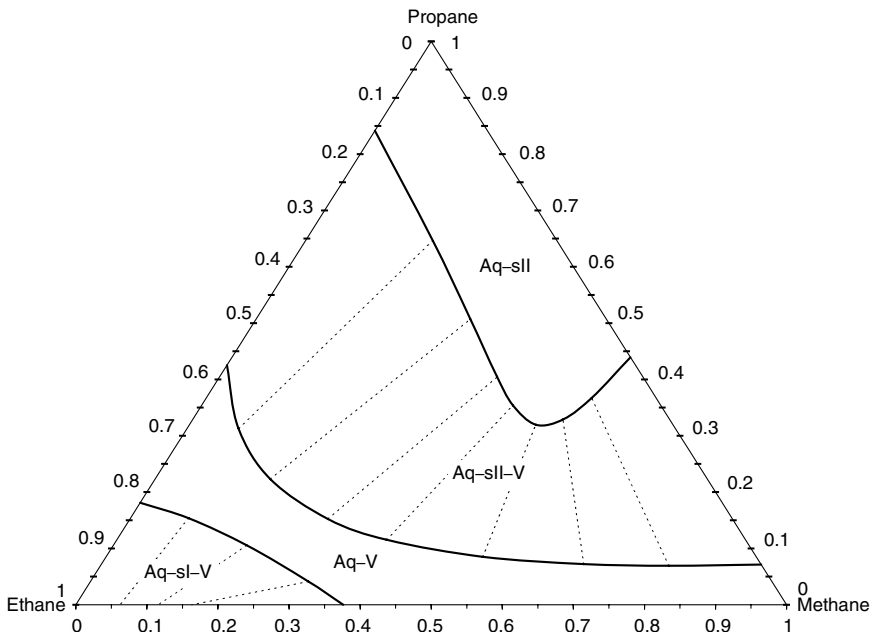


**FIGURE 5.20** Pseudo-ternary diagram for methane + ethane + propane + water system at 277.6 K and 10.13 bar. Ternary diagram scales are component mole fraction.

respectively, and related to the previous binary diagrams. The ethane–propane edge of the phase diagram in Figure 5.20 can be directly compared to the pseudo-*P-x* phase diagram for the ethane + propane + water system in Figure 5.18 at a pressure of 10.13 bar. At 10.13 bar in Figure 5.18, the composition range for the Aq-sII phase region is between 0 and 0.16 mole fraction ethane. This is the same composition range for the Aq-sII phase region on the ethane–propane edge of Figure 5.20. Similar comparisons can be made with each edge of the pseudo-ternary phase diagram and the corresponding pseudo-*P-x* phase diagram (Figure 5.15 for the Methane + Propane pseudo-binary, and Figure 5.16 for the Methane + Ethane pseudo-binary)

The interior of the phase diagram in Figure 5.20 cannot be determined by a simple analysis of the pseudo-phase diagrams. Instead, an example of the procedure to determine the phase equilibria of a given excess water composition of the gas mixture is given. Suppose the excess water composition of the gas mixture is 0.3333 mole fraction for each of the three components. At a temperature and pressure of 277.6 K and 10.13 bar (Figure 5.20), respectively, the overall composition is in the center of the diagram, in the three-phase region (Aq-sII-V). The tie line (dashed line) in Figure 5.20, passing through that overall composition, gives the excess water composition ( $\text{CH}_4$ ,  $\text{C}_2\text{H}_6$ ,  $\text{C}_3\text{H}_8$ ) of the sII hydrate (0.39, 0.19, 0.42) and vapor (0.25, 0.58, 0.17) phases. Note that, because this is a

pseudo-ternary phase diagram with excess water throughout, as is the case of the other diagrams, the composition of water in any of the phases cannot be determined.

The predicted phase diagram in Figure 5.20 indicates that sII hydrate is the predominate hydrate that forms. Propane clearly stabilizes the hydrate over a wide composition range. In Figure 5.20 four major phase regions appear from the top to the bottom of the diagram: Aq-sII, Aq-sII-V, Aq-V, and Aq-sI-V; three of those phase regions contain hydrates and encompass approximately 80% of the overall phase diagram. In other words at a temperature and pressure of 277.6 K and 10.13 bar, respectively, the likelihood of hydrate formation is large given all possible mixture compositions.

For industrial applications, determining the stable hydrate structure at a given temperature, pressure, and composition is not a simple task, even for such a simple systems as the ones discussed here. The fact that such basic mixtures of methane, ethane, propane, and water exhibit such complex phase behavior leads us to believe that industrial mixtures of ternary and multicomponent gases with water will exhibit even more complex behavior. Spectroscopic methods are candidates to observe such complex systems because, as discussed earlier, pressure and temperature measurements of the incipient hydrate structure are not enough.

Experimental work is required to confirm predictions for the majority of these systems at temperatures and pressures above the incipient conditions, and techniques such as diffraction, Raman, and NMR are well suited to do this. Spectroscopic measurements will allow hydrate model parameters to be fit to hydrate composition and structural data. Corrected model predictions can then guide areas to probe experimentally (Subramanian et al., 2000b).

The methane + ethane + propane + water system is the simplest approximation of a natural gas mixture. As shown in Figure 5.20, the phase equilibria of such a simple mixture is quite complicated at pressures above incipient hydrate formation conditions. One of the most interesting phenomenon is the coexistence of sI and sII hydrates which occurs in the interior of some pseudo-ternary phase diagrams.

Chemicals such as kinetic inhibitors or antiagglomerates are added to natural gas pipelines to prevent hydrate plugs. Kinetic inhibitors are designed to slow hydrate formation kinetics while antiagglomerants are designed to prevent hydrate particles from agglomerating. Typical natural gas hydrates are assumed to be sII and therefore these chemicals are designed to prevent sII hydrates from plugging a pipeline. Figure 5.20 suggests that if a natural gas mixture is rich in ethane, sI hydrates will form. With such a structure change it is possible that a kinetic inhibitor or antiagglomerant which may prevent the sII hydrates from plugging the pipeline may not inhibit the sI hydrates which exist at high ethane content.

### 5.3 COMPUTER SIMULATION: ANOTHER MICROSCOPIC–MACROSCOPIC BRIDGE

The major prediction method in this chapter is based on statistical thermodynamics. A statistical sampling of microscopic or molecular properties (e.g., cavities

and their filling by gas molecules) enables the prediction of properties which are macroscopic, or measurable with normal tools such as pressure guages and thermocouples. Although the derivation in Section 5.1 may be somewhat involved, the final equations are simple and are physically related to molecular phenomena.

Physical measurements are directly input to the statistical thermodynamics theory. For example three-phase hydrate formation data, and spectroscopic (Raman, NMR, and diffraction) data were used to determine optimum molecular potential parameters ( $\epsilon$ ,  $\sigma$ ,  $a$ ) for each guest, which could be used in all cavities. By fitting only a eight pure components, the theory enables predictions of engineering accuracy for an infinite number of mixtures in all regions of the phase diagram. This facility enables a substantial savings in experimental effort.

For the first three-quarters of the last century, statistical thermodynamics was the only bridge available between the molecular and the macroscopic domains. However, during the last quarter century, the availability of large, fast digital computers have enabled the use of another technique—namely computer simulation.

In computer simulation, an assembly (or ensemble) of molecules are simulated to predict macroscopic properties. Two simulation techniques have been commonly used, (1) MD and (2) MC. In Section 5.1.9 a third technique, *ab initio* quantum mechanical calculations was shown to provide interatomic potential parameters. In addition lattice dynamics (LD) has been used for the hydrate phase (Sparks and Tester, 1992; Belosludov et al., 1996; Westacott and Rodger, 1997) at considerable savings in computation. A significant LD effort is due to Tanaka and coworkers (Tanaka and Kiyohara, 1993a,b; Koga, 1995, 1994a,b; Koga and Tanaka, 1996) pointing to flaws in the van der Waals and Platteeuw (1959) model.

### 5.3.1 Basic Techniques of Monte Carlo and Molecular Dynamics Simulation

The overview in this section is intended to only provide a brief background for discussion of MD and MC techniques as applied to thermodynamic results. For the reader interested in MD or MC details, [Table 5.11](#) includes a list of standard references. The LD technique, which was originally applied for low temperature solids, will not be considered in this brief overview (see the standard reference in [Table 5.11](#)). Kinetic results for molecular simulations are in [Chapter 3](#).

As with all hydrate theory, it is important to interpret calculations at every opportunity in terms of experiments. With computer simulations, it is deceptively alluring to interpret calculations without physical validation, yet such a path can lead to false conclusions. When physical confirmation is not available, simulations should be regarded with caution. For example, at the heart of both MD and MC methods is the potential energy between individual molecules, which is itself an approximation and limits the accuracy of the simulated macroscopic properties. Such potentials should be validated in terms of their ability to predict measured properties, such as phase equilibria.

**TABLE 5.11**  
**General References for Computer Simulation Techniques**

Author(s)	Title	Publisher	Date
<b>General</b>			
Frenkel, D. and Smit, B.	<i>Understanding Molecular Simulation</i>	Academic Press	2001
<b>Molecular dynamics</b>			
Allen, M.P. and Tildesley, D.J.	<i>Computer Simulation of Liquids</i>	Clarendon Press, Oxford	1989
Gould, H. and Toboshnik, J.	<i>Introduction to Computer Simulation Methods. Applications to Physical Systems, Part 1.</i>	Addison-Wesley	1988
Haile, J.M.	<i>Molecular Dynamics Simulation. Elementary Methods</i>	Wiley & Sons	1992
<b>Monte Carlo</b>			
Gould, H. and Toboshnik, J.	<i>An Introduction to Computer Simulation Methods. Applications to Physical Systems, Part 2.</i>	Addison-Wesley	1988
Kalos, M.H. and Whitlock, P.A.	<i>Monte Carlo Methods., Volume 1: Basics</i>	Wiley & Sons	1986
Rubinstein, R.Y.	<i>Simulation and the Monte Carlo Method</i>	Wiley & Sons	1981
<b>Lattice dynamics</b>			
Horton, G.K. and Maradudin, A.A.	<i>Dynamical Properties of Solids, 3 Volumes</i>	North-Holland Amsterdam	1974

### 5.3.1.1 Molecular dynamics

Molecular dynamics has been used to simulate water structures, wherein an accurate water potential function is used to enable solution of Newton's equations of motion for a small (e.g., 1000–10,000) number of molecules over time. In water and water structures, the SPC (Berendsen et al., 1981) and the TIP4P (Jorgensen et al., 1983) potential models are most often used. Reanalysis of extant diffraction data by Soper et al. (1997) has called both of these potentials into question.

The integration of forces between all molecules over several thousand time-steps produces particle trajectories from which time-averaged macroscopic properties can be computed. In MD the simulation is limited by the computer storage capacity and speed, so that short-lived phenomena (100–1000 ps) are generally calculated.

Compared to MC, the MD technique is used more often, perhaps because it can calculate time-dependent phenomena and transport properties such as viscosity, thermal conductivity, and diffusivity, in addition to thermodynamic properties. However, Haile, (1992, p. 17) states a criterion for calculation of time-dependent

properties:

the relaxation time for the phenomenon under investigation must be small enough so that one simulation generates several relaxation times

Times for molecular dynamic calculations are thus not well suited for calculation of hydrate kinetic nucleation phenomena, which can have metastability lasting hours or days, while the simulation is typically limited to  $10^{-9}$  s.

The molecular dynamic technique has been validated for water structures through comparison of calculated properties with experimental thermodynamic water data, such as the density maximum, the high heat capacity, and diffraction patterns (Stillinger and Rahman, 1974) as well as the hydrate infrared (vibrational) spectral data by Bertie and Jacobs (1977, 1982). With acceptable comparisons of many computed and experimental properties of water structures, there is little doubt that a substance similar to water has been simulated.

Work in three laboratories comprises most of the MD hydrate studies. The pioneering works of Tse and coworkers (1983a,b, 1984, 1987) are exemplary in comparing simulation calculations to measurements, principally through macroscopic or spectroscopic techniques. The recent work of Tse et al. (1997) suggests limits to the use of infrared and Raman instruments due to enclathration changes of guest electronic and vibrational properties.

The second major study in MD was made by Rodger and coworkers (1989, 1990a,b, 1991) who considered structural stability. A third significant effort (including the aforementioned LD work) comes from Tanaka and coworkers (1993a,b; Koga et al., 1994a,b, 1996). Some conclusions from these studies are discussed in the Section 5.3.2.

Molecular dynamic studies in Holder's laboratory (Hwang, 1989; Hwang et al., 1993; Zele, 1994) have calculated Langmuir coefficients, such as in Equation 5.27 and considered the effect of guests which stretch the host lattice. Work in this laboratory concentrated on the clustering of water around guest molecules (Long and Sloan, 1993) and system behavior at the hydrate–water interface (Pratt and Sloan, 1995). Wallqvist (1991, 1992, 1994a,b) considered clustering, and the thermodynamic inhibitor methanol inside the hydrate cage.

Itoh et al. (1996) used MD to explain the CO<sub>2</sub> bending and stretching peaks in Raman spectra. Recently Carver et al. (1995), Kvamme et al. (1996), Makogon (1997), and Anderson (2005) used MD to model hydrate kinetic inhibitors interactions with the crystal surface.

### 5.3.1.2 Monte Carlo

The universal algorithm of MC methods was provided early after computers came into use by Metropolis et al. (1953). The name MC stems from a random number generator in the method, similar to that used in casinos.

In the MC method, molecules are moved randomly from an initial configuration, so that only the immediately previous configuration affects the current position. Using the individual potential (e.g., SPC or TIP4P) between

each particle, the total energy  $U$  is computed for the new configuration and compared with the previous value. If  $U_{\text{new}} < U_{\text{old}}$ , the move is accepted; however, if  $U_{\text{new}} > U_{\text{old}}$ , the change is accepted with a probability proportional to the Boltzmann distribution [ $\exp(-\Delta U/kT)$ ].

In each new configuration thermodynamic properties are calculated, and accumulated in running sums, usually over a few million configurations. The space average from MC is the same as the MD time average of thermodynamic properties, confirming the Ergodic Hypothesis in statistical mechanics, that all of phase space is sampled representatively, given a large enough sample size. However, because MC techniques are limited to time-independent properties, they have not been used as extensively as molecular dynamic techniques.

As in the molecular dynamic calculations, MC calculations for water structures were first tested against experimental values. Beveridge and coworkers (Swaminathan et al., 1978) and Owicky and Scheraga (1977) obtained acceptable comparison of their calculations against experimental values for the oxygen–oxygen radial distribution function for both water and methane dissolved in water.

There are substantially fewer MC studies of hydrates than there are MD studies. The initial MC study of hydrates was by Tester et al. (1972), followed by Tse and Davidson (1982), who checked the Lennard-Jones–Devonshire spherical cell approximation for interaction of guest with the cavity. Lund (1990) and Kvamme et al. (1993) studied guest–guest interactions within the lattice. More recently Natarajan and Bishnoi (1995) have studied the technique for calculation of the Langmuir coefficients.

### 5.3.2 What has been Learned from Molecular Simulation?

Here we list some of the most significant applications of molecular simulation, as provided by Wierzchowski (Personal Communication, October 4, 2006) although this list is by no means exhaustive. Since the first applications of molecular simulation to hydrates by Tse, et al. (1983a,b; 1984), the tool has been widely used to interpret physical behavior. Simulation has impacted six major hydrate research areas.

1. Stability. Rodger (1990a,b,c) was first to note the utility of molecular simulation to investigate the van der Waals and Platteeuw statistical mechanical theory. The study argues the importance of repulsive forces from the guest molecules on stabilizing the hydrate water lattice. Tanaka and co-workers (Tanaka and Kiyohara, 1993a,b; Tanaka, 1994; Tanaka et al., 2004) enabled the understanding of hydrate stability via LD. The work extends over a decade, probing concepts related to non-spherical guest molecules (Tanaka, 1994), double hydrate stability (Tanaka et al., 2004), and double occupancy of cages (Tanaka, 2005).

2. Nucleation. Understanding the phenomena of nucleation is a central concept to developing a hydrate formation model. As detailed in [Chapter 3](#), Radhakrishnan and Trout (2002) used a new simulation technique to formulate a concept of hydrate

progression from liquid to a crystal state, indicating the critical cluster diameter for CO<sub>2</sub> hydrate nucleation is 9.6–14.5 Å. Methane hydrate nucleation was analyzed by Baez and Clancy (1994) and Moon et al. (2003), observing formation of methane hydrate clusters.

3. Kinetic inhibitors. The advent of kinetic inhibitors stimulated simulation in molecular design (Freer and Sloan, 2000) and understanding functional groups (Carver et al., 1995). Recently, simulation was employed to screen quaternary ammonium zwitterions (Storr et al., 2004). Moreover, Anderson et al. (2005) detailed kinetic inhibitors binding energies to methane hydrates. Both studies showed a correlation between the inhibitor functional groups and the charge distribution of a hydrate surface.

4. Interfacial properties. The behavior of hydrate molecules at the surface of a hydrate is central to hydrate agglomeration and crystal growth. Rodger et al. (1996) applied simulation to investigate the stiffness and motion of molecules at the methane hydrate/methane gas interface. As a result, an intermediate region (liquid-like/hydrate-like) at the hydrate surface was identified. Almost at the same time, the interface of structure H hydrate was investigated by Pratt and Sloan (1996), detailing the translation and orientation effects of molecules at the hydrate/water interface.

5. Spectral properties. The inaugural hydrate simulations of Tse et al. (1983a,b, 1983, 1984) demonstrated the utility of MD in studying spectral properties. The tool is effective in deciphering spectra from encaged molecules, and subsequently Tse (1994) revealed three characteristic frequencies of methane vibrations (in methane hydrate) are in accord with neutron scattering data (Sears et al., 1992). Later, Itoh et al. (2000) simulated intramolecular vibrational spectra of methane, showing the stretching mode of methane and comparing with experimental findings.

6. Anomalous properties—thermal expansivity and thermal conductivity. Molecular simulation has been integral in evaluating physical behaviors of hydrate compared with ice, specifically a larger thermal expansivity (Tse, et al., 1987; Tanaka, et al., 1997) and a glasslike thermal conductivity (Tse, et al., 1983; 1984; Inoue, et al., 1996). These properties have been explained by the coupling between the water and the guest molecules.

In summary, the MD, MC, and LD (lattice dynamic) techniques are very powerful tools to investigate hydrate phenomena. Indeed, hydrate computer simulations may shortly outnumber hydrate experimental observations, because simulations are generally more accessible than experiments. However, such tools investigate phenomena which are on much smaller time and space dimensions than normally observed, outside of spectroscopy. Even with spectroscopy, the relevant peaks may be subject to some interpretation. As a result there may be several microscopic interpretations (based upon hundreds to thousands of molecules) of macroscopic phenomena which involve typically 10<sup>23</sup> molecules. Such a scale-up may cause misinterpretation.

Computer simulation is best done (1) to propose experimental phenomena usually not accessible due to size or time scales, or (2) to explain experimental observation. The best simulation predictions are done jointly with experimental confirmation.

## 5.4 CHAPTER SUMMARY AND RELATIONSHIP TO FOLLOWING CHAPTERS

The statistical thermodynamic method and the Gibbs energy minimization presented in this chapter represents the state-of-the-art for the prediction of the following types of phase equilibria:

1. Compressible three-phases ( $L_w-H-V$  or  $I-H-V$ )
2. Incompressible three-phases ( $L_w-H-L_{HC}$ )
3. Inhibition of equilibria in (1) or (2)
4. Quadruple points/lines ( $L_w-H-V-L_{HC}$  or  $I-L_w-H-V$ )
5. Two-phase ( $H-V$  or  $H-L_{HC}$ ) equilibria
6. Four and five phase equilibria of structure H
7. Flash calculations
8. Expansion through a valve or turbine

The CSMGem computer program and Users Manual on the disk with this book (and the program examples in [Appendix A](#)) enables prediction of such properties using the methods of this chapter. The method has been shown to predict interesting results in the single, binary, and ternary phase diagrams of methane + ethane + propane, including retrograde phenomena, which was subsequently confirmed via experiment.

By comparing the program predictions with data, along with those of three current commercial hydrate programs, the conclusion is reached that the current state-of-the-art programs can predict the uninhibited, incipient hydrate formation temperature and pressure to within an average of 0.65 K and 10% of overall pressure, respectively. The equivalent inhibited inaccuracies for incipient temperature and pressure are 2 K and 20% in overall pressure, respectively.

The chapter also examined three molecular methods: (1) *ab initio* quantum mechanical calculations, which are typically used to get better interatomic potentials, (2) MC calculations, and (3) molecular dynamic calculations. The latter two molecular methods are most useful to probe the behavior of a small number of molecules, in which experimental capability is constrained by either space or time.

[Chapter 6](#), which immediately follows, presents experimental methods and data for comparison with predictions in the present chapter. Such data will form the foundation for future modifications of theory in hydrate phase equilibria. However, the above thermodynamic prediction accuracies are usually satisfactory for engineering calculations, so that the state-of-the-art in hydrates is turning from thermodynamic (time-independence) to kinetics (time-dependence) phenomena,

such as those in [Chapter 3](#). In science and engineering, kinetic prediction methods are typically an order of magnitude less accurate than thermodynamic properties, due to the additional variable of time.

[Chapter 7](#) then considers the formation of hydrates in nature, such as in the permafrost and deep oceans of the earth. In such situations geologic time mitigates the necessity for kinetic formation effects and allows the use of thermodynamic conditions, such as those in the three-phase portions of the present chapter, for identification, exploration, and recovery.

[Chapter 8](#) presents problems of natural gas production, transportation, and processing which are related to hydrates. Because a standard kinetic treatment method has progressed past the fledgling state in the second edition (1998), the state-of-the-art in flow assurance is turning away from thermodynamic properties which encourage hydrate avoidance, to kinetic properties which encourage a new philosophy in flow assurance—that of risk management.

## REFERENCES

- Anderson, B., *Molecular Modeling of Clathrate-Hydrates via Ab-Initio, Cell Potential and Dynamic Methods*, Massachusetts Institute of Technology, MA (2005).
- Anderson, B.J., Tester J.W., Borghi, G.P., Trout, B.L., *J. Am. Chem. Soc.*, **127**, 17852 (2005).
- Avlonitis, D., *Chem. Eng. Sci.*, **49**, 1161 (1994).
- Baez, L.A., Clancy, P.A., in (*First*) *Int. Conf. on Natural Gas Hydrates* (Sloan, E.D., Happel, J., Hnatow, M.A., eds.), *Ann. N.Y. Acad. Sci.*, **715**, 177 (1994).
- Baker, L.E., Pierce, A.C., Luks, K.D., *J. Soc. Pet. Eng.*, 731 October (1982).
- Ballard, A.L., *A Non-Ideal Hydrate Solid Solution Model for a Multiphase Equilibria Program*, Ph.D. Thesis, Colorado School of Mines, Golden, CO (2002).
- Ballard, A.L., Jager, M.D., Nasrifar, Kh., Mooijer-van den Heuvel, M.M., Peters, C.J., Sloan, E.D., *Fluid Phase Equilib.*, **185**, 77 (2001).
- Ballard, A.L., Sloan, E.D., *Chem. Eng. Sci.*, **56**, 6883 (2001).
- Ballard, A.L., Sloan, E.D., *Fluid Phase Equilib.*, **371**, 194–197 (2002a).
- Ballard, A.L., Sloan, E.D., *J. Supramol. Chem.*, **2**, 385–392 (2002b).
- Ballard, A.L., Sloan, E.D., *Fluid Phase Equilib.*, **218**, 15–31 (2004a).
- Ballard, A.L., Sloan, E.D., *Fluid Phase Equilib.*, **216**, 257–270 (2004b).
- Barrer, R.M., Stuart, W.I., *Proc. R. Soc. (London) A.*, **243**, 172 (1957).
- Bazant, M.Z., Trout, B.L., *Physica A*, **300**, 139 (2001).
- Belosludov, R., Grachev, E., Dyadin, Y., Belosludov, V., in *Proc. Second International Conference on Natural Gas Hydrates*, (Monfort, J.P., ed.), Toulouse, France, 2–6 June, 303 (1996).
- Berendsen, J.D., Postma, J.P.M., van Gasteren, W.F., Herman, J., in *Intermolecular Forces*, (Pullman, B., ed.), Reidel, Dordrecht (1981).
- Bertie, J.E., Jacobs, S.M., *Can. J. Chem.*, **55**, 1777 (1977).
- Bertie, J.E., Jacobs, S.M., *J. Chem. Phys.*, **77**, 3230 (1982).
- Cady, G.H., *J. Phys. Chem.*, **85**, 4437 (1983a).
- Cady, G.H., *J. Chem. Educ.*, **60**, 915 (1983b).
- Cao, Z., *Modeling of Gas Hydrates from First Principles*, Ph.D. Thesis, Massachusetts Institute of Technology (2002).

- Carver, T.J., Drew, M.G.B., Rodger, P.M., *J. Chem. Soc. Faraday Trans.*, **91**, 3449 (1995).
- Davidson, D.W., *Can. J. Chem.*, **49**, 1224 (1971).
- Davidson, D.W., in *Water: A Comprehensive Treatise*, Plenum Press, New York, **2**, Chapter 3, 115 (1973).
- Davidson, D.W., Ripmeester, J.A., in *Inclusion Compounds* (Atwood, J.L., Davies, J.E.D., MacNichol, D.D., eds.), Academic Press, **3**, Chapter 3, London, U.K. (1984).
- de Loos, Th.W., *Appl. Sci.*, **273**, 89 (1994).
- DePriester, C.L., *Chem. Eng. Prog. Symp. Ser.*, **49**(7), 1 (1953).
- Fowler, R.H., Guggenheim, E.A., *Statistical Thermodynamics*, Cambridge University Press, Cambridge, U.K. (1952).
- Freer, M.E., Sloan, E.D., *Ann. N.Y. Acad. Sci.* (Holder, G.D., Bishnoi, P.R., eds.), **912**, 651 (2000).
- Gibbs, J.W., *The Collected Works of J. Willard Gibbs, Thermodynamics*, **I**, 55–353, Yale University Press, New Haven, Connecticut (1928).
- Gupta, A.K., *Steady State Simulation of Chemical Processes*, Ph.D. Thesis, University of Calgary, Alberta (1990).
- Hadden, S.T., Grayson, H.G., *Hydrocarbon Proc. Petrol. Refiner.*, **40**, 207 (1961).
- Haile, J.M., *Molecular Dynamics Simulations: Elementary Methods*, John Wiley & Sons, Inc., New York (1992).
- Hill, T.L., *An Introduction to Statistical Thermodynamics*, Addison-Wesley, Reading, MA (1960).
- Holder, G.D., *Multi-Phase Equilibria in Methane–Ethane–Propane–Water Hydrate Forming Systems*, Ph.D. Thesis, University of Michigan, University Microfilms No. 77-7939, Ann Arbor, MI 48106 (1976).
- Holder, G.D., Hand, J.H., *AICHE J.*, **28**, 44 (1982).
- Holder, G.D., Manganiello, D.J., *Chem. Eng. Sci.*, **37**, 9 (1982).
- Huo, Z., *Hydrate Phase Equilibria Measurements by X-Ray Diffraction and Raman Spectroscopy*, Ph.D. Thesis, Colorado School of Mines, Golden, CO (2002).
- Hwang, M.J., *A Molecular Dynamic Simulation Study of Gas Hydrates*, Ph.D. Thesis, University of Pittsburgh, Pittsburgh, PA (1989).
- Hwang, M.J., Holder, G.D., Zele, S.R., *Fluid Phase Equil.*, **93**, 437 (1993).
- Inoue, R., Tanaka, H., Nakanishi, K., *J. Chem. Phys.*, **104**, 9569 (1996).
- Itoh, H., Kawamura, K., *Ann. N.Y. Acad. Sci.* (Holder, G.D., Bishnoi, P.R., eds.), **912**, 693 (2000).
- Jager, M.D., Ballard, A.L., Sloan, E.D., *Fluid Phase Equilib.*, **211**, 85–107 (2003).
- Jorgensen, W.L., Chandrasekhar, J., Madura, J.D., Impey, R.W., Klein, M.L., *J. Chem. Phys.*, **79**, 926 (1983).
- Kihara, T., *J. Phys. Soc. Japan*, **6**, 289 (1951).
- Klauda, J.B., *Ab initio Intermolecular Potentials to Predictions of Macroscopic Thermodynamic Properties and the Global Distribution of Gas Hydrates*, Ph.D. Thesis, University of Delaware, 2003.
- Koga, K., *Study of Stability and Dynamics of Clathrate Hydrates and Supercritical Fluids*, Ph.D. Thesis, Kyoto University, Japan (1995).
- Koga, K., Tanaka, H., *J. Chem. Phys.*, **104**, 263 (1996).
- Koga, K., Tanaka, H., Nakanishi, K., *J. Chem. Phys.*, **101**, 3127 (1994a).
- Koga, K., Tanaka, H., Nakanishi, K., *Mol. Simul.*, **12**(3–6), 241 (1994b).
- Kvamme, B., Juseby, G., Forrisdahl, O., in *Proc. Second International Conference on Natural Gas Hydrates*, (Monfort, J.P., ed.), Toulouse, France, June 2–6, 347 (1996).
- Kvamme, B., Lund, A., Hertzberg, T., *Fluid Phase Equilib.*, **90**, 15 (1993).

- Lennard-Jones, J.E., Devonshire, A.F., *Proc. R. Soc. A*, **163**, 53 (1932).
- Lennard-Jones, J.E., Devonshire, A.F., *Proc. R. Soc. A*, **165**, 1 (1938).
- Lewis, G.N., Randall, M., *Thermodynamics*, McGraw-Hill Book Co., New York, 1923.
- Lund, A., The Influences of Gas-Gas Interactions on the Stability of Gas Hydrates, Ph.D. Thesis, Norwegian Technical University.
- Mak, T.C.W., McMullan, R.K., *J. Chem. Phys.*, **42**, 2732 (1965).
- Makogon, T.Y., *Kinetic Inhibition of Natural Gas Hydrates Formation*, Ph.D. Dissertation, Colorado School of Mines, Golden, CO (1997).
- Makogon, Y.F., *Hydrates of Natural Gas*, Moscow, Nedra, Izdatelstro, p. 208 (1974 in Russian) Transl W.J. Cieslesicz, PennWell Books, Tulsa, Oklahoma p. 237 in Russian, (1981 in English).
- McKoy, V., Sinanoglu, O., *J. Chem. Phys.*, **38**, 2946 (1963).
- McMullan, R.K., Jeffrey, G.A., *J. Chem. Phys.*, **42**, 2725 (1965).
- McQuarrie, D.A., *Statistical Mechanics*, Harper & Row, New York (1976).
- Metropolis, N., Riosenbluth, A.W., Rosenbluth, M.N., Teller, A.H., Teller, E., *J. Chem. Phys.*, **21**, 1087 (1953).
- Moon, C., Taylor, P.C., Rodger, P.M., *J. Am. Chem. Soc.*, **125**, 4706 (2003).
- Natarajan, V., Bishnoi P.R., *Ind. Eng. Chem. Res.*, **34**, 1494 (1995).
- Owicki, J.C., Scheraga, H.A., *J. Am. Chem. Soc.*, **99**, 7413 (1977).
- Parrish, W.R., Prausnitz, J.M., *Ind. Eng. Chem. Proc. Des & Dev.*, **11**, 26 (1972).
- Pratt, R.M., Sloan, E.D., *Mol. Simul.*, **15**, 247 (1995).
- Rachford, H.H., Rice, J.D., *J. Pet. Technol.*, **4**(p. 10), 1(p. 19), **2**(p. 3) (1952).
- Radhakrishnan, R., Trout, B.L., *J. Chem. Phys.*, **117**, 1786 (2002).
- Rodger, P.M., *J. Phys. Chem.*, **93**, 6850 (1989).
- Rodger, P.M., *Chem. Br.*, 1090, November (1990a).
- Rodger, P.M., *J. Phys. Chem.*, **94**, 6080 (1990b).
- Rodger, P.M., *AIChE J.*, **37**, 1511 (1991).
- Rodger, P.M., Forester, T.R., Smith, W., *Fluid Phase Equilib.*, **116**, 326 (1996).
- Rowley, R.L., *Statistical Mechanics for Thermophysical Property Calculations*, Prentice Hall, Englewood Cliff, NJ (1994).
- Sears, V.J., Powell, B.M., Tse, J.S., Ratcliffe, C.I., Handa, Y.P., *Physica*, **B181**, 658 (1992).
- Sloan, E.D., *Fluid Phase Equilib.*, **228–229C**, 67 (2005).
- Soper, A.K., Bruni, F., Ricci, M.A., *J. Chem. Phys.*, **106**(1), 247 (1997).
- Sparks, K.A., Tester, J.W., *J. Phys. Chem.*, **96**, 11022 (1992).
- Stillinger, F.H., Rahman, A., *J. Chem. Phys.*, **60**, 1545 (1974).
- Storr, M.T., Taylor, P.C., Monfort, J.P., Rodger, P.M., *J. Am. Chem. Soc.*, **126**, 1569 (2004).
- Subramanian S., Kini, R., Dec, S.F., Sloan, E.D., *Chem. Eng. Sci.*, **55**, 198 (2000a).
- Subramanian, S., Ballard, A.L., Kini, R., Dec, S.F., Sloan, E.D., *Chem. Eng. Sci.*, **55**, 5763 (2000b).
- Swaminathan, S., Harrison, S.W., Beveridge, D.L., *J. Am. Chem. Soc.*, **100**, 5705, (1978).
- Tanaka, H., *J. Chem. Phys.*, **101**, 10833 (1994).
- Tanaka, H., Kiyohara, K., *J. Chem. Phys.*, **98**, 8110 (1993a).
- Tanaka, H., Kiyohara, K., *J. Chem. Phys.*, **98**, 4098 (1993b).
- Tanaka, H., Nakatsuka, T., Koga, K., *J. Chem. Phys.*, **121**, 5488 (2004).
- Tanaka, H., Tamai, Y., Koga, K., *J. Phys. Chem. B*, **101**, 6560 (1997).
- Tester, J.W., Bivins, R.L., Herrick, C.C., *AIChE J.*, **18**(6), 1220 (1972).
- Tse, J.S., *J. Incl. Phenom.*, **8**, 25 (1990).
- Tse, J.S., *Ann. N.Y. Acad. Sci.* (Sloan, E.D., Happel, J., Hnatow, M.A., eds.), **715**, 187 (1994).

- Tse, J.S., Davidson, D.W., *Proc 4<sup>th</sup> Can. Perm. Conf.*, p. 329, Calgary, Alberta, March 2–6, 1981 (1982).
- Tse J.S., Klein, M.L., McDonald, I.R., *J. Chem. Phys.*, **78**, 2096 (1983a).
- Tse, J.S., Klein, M.L., McDonald, I.R., *J. Phys. Chem.*, **87**, 4198 (1983b).
- Tse J.S., Klein, M.L., McDonald, I.R., *J. Chem. Phys.*, **81**, 6146 (1984).
- Tse, J.S., McKinnon, W.R., Marchi, M., *J. Phys. Chem.*, **91**, 4188 (1987).
- van der Waals, J.H., Platteeuw, J.C., *Adv. Chem. Phys.*, **2**, 1 (1959).
- von Stackelberg, M., Jahns, W., *Z. Electrochem.*, **58**, 162 (1954).
- Wallqvist, A., *Chem. Phys. Lett.*, **182(3, 4)**, 237 (1991).
- Wallqvist, A., *J. Chem. Phys.*, **96**, 5377 (1992).
- Wallqvist, A., in (*First*) *Int. Conf. on Natural Gas Hydrates*, *Ann. N.Y. Acad. Sci.*, (Sloan, E.D., Happel, J., Hnatow, M.A., eds.), **715**, 159, (1994a).
- Wallqvist, A., in (*First*) *Int. Conf. on Natural Gas Hydrates*, *Ann. N.Y. Acad. Sci.*, (Sloan, E.D., Happel, J., Hnatow, M.A., eds.), **715**, 540, (1994b).
- Westacott, R.E., Rodger, P.M., “Direct Free Energy Calculations for Gas Hydrates,” in *Proc. 213th ACS National Meeting*, San Francisco, CA, April 13–17, **42(2)** 539 (1997).
- Wilcox, W.I., Carson, D.B., Katz, D.L., *Ind. Eng. Chem.*, **33**, 662 (1941).
- Zele, S.R., *Molecular Dynamics and Thermodynamic Modeling of Gas Hydrates*, Ph.D. Thesis, University of Pittsburgh, Pittsburgh, PA (1994).